EE

DESY 94-243
December 1994

On a Possibility to Construct Gamma-Gamma Collider at TESLA

hep-ex/9503

E. L. Saldin, E. A. Schneidmiller, Yu. N. Ulyanov
Automatic Systems Corporation, Samara, Russia
V. P. Sarantsev, M. V. Yurkov
Joint Institute for Nuclear Research, Dubna, Moscow Region, Russia

ISSN 0418-9833

DESY 94-243
December 1994

ISSN 0418-9833

On a Possibility to Construct Gamma-Gamma Collider at TESLA

E.L. Saldin [b], V.P. Sarantsev [a], E.A. Schneidmiller [b], Yu.N. Ulyanov [b] and M.V. Yurkov [a]

[a] *Joint Institute for Nuclear Research, Dubna, 141980 Moscow Region, Russia*

[b] *Automatic Systems Corporation, 443050 Samara, Russia*

Abstract

This paper presents the conceptual project of a 2 × 250 GeV photon collider at TESLA. The main idea of the proposal is to use the beam of the linear collider to generate FEL radiation. At an intermediate phase of acceleration ($\mathcal{E}$ = 10 GeV) the electron beam passes the undulator of the FEL amplifier and amplifies the optical radiation of the master oscillator ($\lambda = 1.053\ \mu$ m, peak power 100 MW). An output radiation of 350 GW peak power is produced at the amplifier exit. After that the electron and optical bunches are separated. The electron bunch is accelerated up to the final energy of 250 GeV and the optical bunch is transported to the conversion point via an open optical waveguide which has the form of a diaphragm focusing line and is placed in parallel with the main accelerator. At the conversion point the optical beam is focused on the electron beam and after the conversion point the gamma quanta follow the initial electron trajectory and meet at the interaction point with the other gamma-beam produced by another part of the collider. The integral luminosity of the colliding γ-beams is $L_{\gamma\gamma} \simeq 1.5 \times 10^{33}\ \mathrm{cm}^{-2}\mathrm{s}^{-1}$.

The feasibility of the proposal is confirmed by the results of numerical simulations.

Preprint submitted to Elsevier Science *22 December 1994*

1 Introduction

It is evident nowadays that traditional circular e^+e^- colliders exhausted their capabilities to attain a center-of-mass energy higher than 200 GeV. So, this energy region could be exploited only with the future generation of linear colliders. It is assumed that the first linear colliders will operate in the center-of-mass energy of about 500 GeV [1]. In addition to providing electron-positron colliding beams, linear colliders can reveal an unique opportunity to study the structure of matter by means of colliding photon-photon or photon-electron (positron) beams. For instance, topponium $C = +1$ states could be studied in two-photon reactions. The Higgs bosons could also be produced using photon colliding beams via the branch $\gamma\gamma \to H$. Even in the case when the Higgs boson will be found at e^+e^- linear colliders, its properties may be studied in detail only with photon linear colliders [2].

The idea to construct a photon linear collider (PLC) is based on a peculiar feature of the linear collider, namely that electron (positron) beams are used only once during the duty cycle of the collider and are dumped after interaction. It was proposed in the early 80's to convert the energy of electrons into high energy γ-quanta and to organize collision of the high energy γ-beams [3,4]. From technical point of view the construction of the photon linear collider seems to be more simple. First, there is no need for positrons for the PLC operation, so the injection system of the collider can be simplified significantly. For instance, the damping ring can be removed and the injection system could be built on the basis of the photoinjector technique. Secondly, the problems connected with beam-beam interaction are not so severe as in the case of the colliding electron-positron beams, so there is no need to prepare flat beams and round beams can be used. On the other hand, a novel problem arises, namely that of an effective conversion of electrons into high energy γ-quanta.

It is accepted now that the use of Compton backscattering of laser light on the electrons of the collider is the optimal way to solve this problem. It is likely that the laser light wavelength should be tunable as there exists an optimal value of the laser light wavelength which depends on the energy of the electrons $\mathcal{E}$ as $\lambda\ (\mu\text{m}) \simeq 4 \times \mathcal{E}\ (\text{TeV})$ [1]. For instance, if the energy of the electrons is equal to 250 GeV, the laser light wavelength should be of about 1 μm. To provide high conversion efficiency, the peak power of the laser must be rather high. For instance, to achieve 70 % conversion efficiency, the peak power of the laser should be about 300 GW (this value corresponds to a laser with an ideal, i.e. diffraction dispersion, otherwise the peak power

[1] At a shorter wavelength, the process of e^+e^- pair production begins to play a significant role, thus increasing the background. At a longer wavelength, the maximal energy of γ-quanta is decreased [5].

must be higher). The laser pulse format must follow the pulse format of the electron bunches of the linear collider. It means, that the laser should have the capability of precise synchronization with the electron bunches (with the jitter of about 1 ps) and should provide a high repetition rate. To provide a wider range of physical experiments, there should be a possibility to steer the polarization of the colliding gamma quanta which assumes a possibility to steer the polarization of the laser light.

An analysis of existing quantum lasers shows that all these requirements can not be fulfilled simultaneously. As for the peak radiation power, they are capable to generate peak output power $\sim$ 1 TW with the required pulse duration. As for the repetition rate, it can not be achieved due to the low efficiency of quantum lasers and the problem to cool the active medium.

On the other hand, the free electron laser (FEL) technique provides a possibility to construct the laser system which meets all the requirements for the PLC. Indeed, the FEL can provide a high efficiency, it is tunable and capable to generate powerful coherent radiation which always has minimal (i.e. diffraction) dispersion. With a sufficient quality of the driving electron beam, the FEL peak output power is defined by the peak power of this driving beam. At an electron beam energy of $\mathcal{E} \sim 1$ GeV and a peak beam current of $I \sim 1$ kA, this power reaches the TW level. The problem of synchronization can be solved naturally as it is based totally on the accelerator-technology. The FEL output radiation is totally polarized: circularly or linearly for the case of helical or planar undulator, respectively. This feature of the FEL radiation reveals wide possibilities to steer the helicity and energy spectrum of colliding gamma quanta (see Appendix A).

The idea to use the FEL in the PLC scheme was proposed in ref. [4]. Later this approach has been developed in refs. [6,7] where different aspects of the FEL based photon linear colliders have been discussed. In ref. [6] we have studied the possibility of constructing a high-luminosity 2×5 GeV photon collider at SLC. It was shown that construction of such a collider with luminosity up to $10^{34}\mathrm{cm}^{-2}\mathrm{s}^{-1}$ is quite possible with a minor upgrade of the existent SLC facility. In ref. [7] we have considered conceptual projects of the FEL based PLC in the TeV energy range and we have shown that FEL systems for PLC application can be constructed at the present level of accelerator technology.

In the present paper we study the possibility to construct the PLC on the basis of the superconducting collider TESLA [1]. The general parameters of the TESLA collider are presented in Table 1 [1]. The repetition rate of the collider is 10 Hz and 800 bunches of 6 ps pulse duration are accelerated within each macropulse. To construct a photon linear collider on the basis of TESLA, one needs to construct a laser with a wavelength of about 1 μm and a peak power of about 300 GW which possesses the capability to provide the necessary

Table 1
Main parameters for the e^+e^- version of the TESLA project at 2 x 250 GeV

Beam energy, GeV	250
Gradient, MV/m	25
Two-linac active length, km	20
RF frequency, GHz	1.3
Number of particles per bunch	5.14×10^{10}
Number of bunches per pulse	800
Bunch separation, μs	1
Repetition frequency, Hz	10
R.M.S. bunch length σ_z, cm	0.1
Luminosity, $cm^{-2}s^{-1}$	2.6×10^{33}

time diagram of operation.

Our investigation has shown that the project parameters of TESLA allow one to use the electron beam of the main accelerator at an intermediate stage of acceleration (10 GeV) as the driving beam for the FEL amplifier. Such an FEL amplifier is capable to produce the photon beam characteristics which meet the requirements for the PLC applications. It was shown also that the TESLA Test Facility could be used as a test basis for a photon linear collider design.

2 Conceptual project of the PLC

In this section we present the conceptual project of a 2 x 250 GeV photon collider at TESLA. A scheme of this collider is presented in Figs.1 and 2 and its parameters are summarized in Table 2. The main idea of the proposal is to use the beam of the linear collider to generate radiation. At the intermediate phase of acceleration ($\mathcal{E}$ = 10 GeV) the electron beam passes the undulator of the FEL amplifier and amplifies the optical radiation from the master oscillator ($\lambda = 1.053$ μ m, peak power 100 MW). An output radiation of 350 GW peak power is produced at the amplifier exit. Then the electron and optical bunches are separated. The electron bunch is accelerated up to the final energy of 250 GeV and the optical bunch is transported to the conversion point via an open optical waveguide which has the form of a diaphragm focusing line and which is placed in parallel with the main accelerator. To provide optimal focusing conditions at the conversion point, the optical bunch should advance

the electron bunch by several tens of centimeters. This is provided by an optical delay line with the delay time equal to the time interval between bunches. In this case the radiation generated by one bunch is focused on the following one. After the conversion point the gamma quanta follow the initial electron trajectories and meet in the interaction point with the other gamma-beam produced by the opposite part of the collider. The integral luminosity of the colliding γ-beams is $L_{\gamma\gamma} \simeq 1.5 \times 10^{33}$ cm^{-2}s^{-1}.

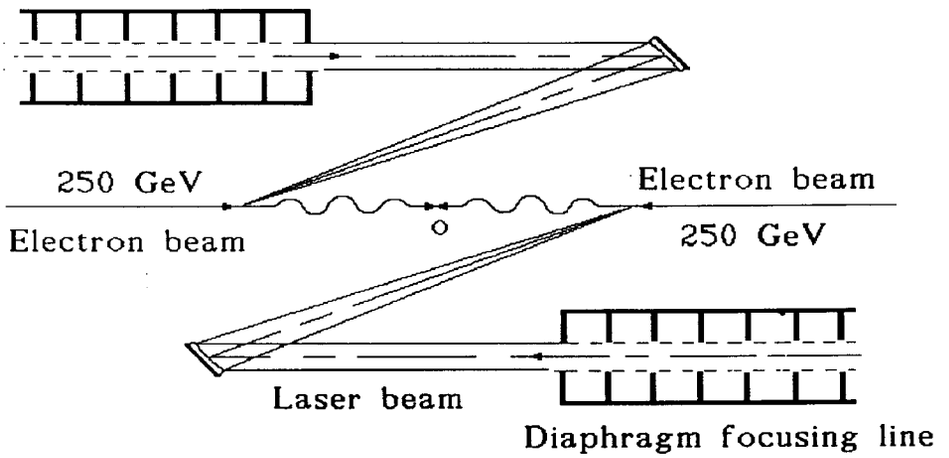

Fig. 1. Conceptual scheme of the photon linear collider at TESLA

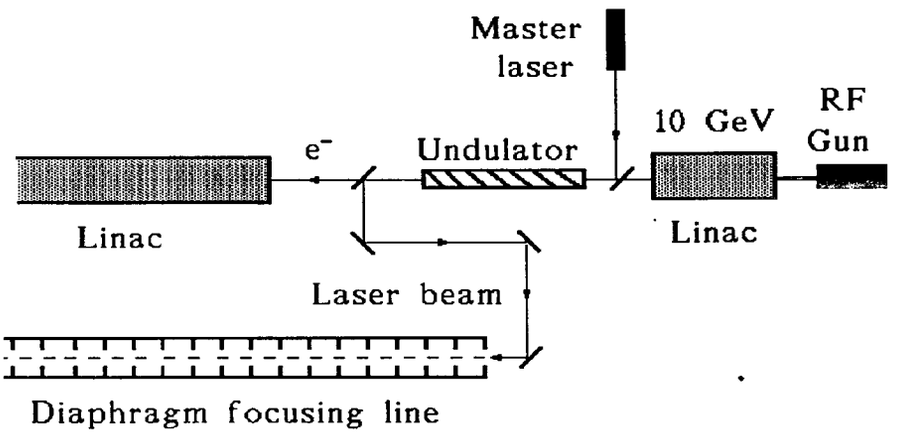

Fig. 2. Conceptual scheme of an FEL amplifier for the photon linear collider at TESLA

Such an approach naturally provides the synchronization of the optical and laser bunches and the generation of the laser beam with the required pulse duration and repetition rate.

Table 2
Main parameters for a $\gamma\gamma$ version of the TESLA project

Main linear accelerator	
Electron beam energy, GeV	250
Number of electrons per bunch	5.14×10^{10}
Number of bunches per pulse	800
Bunch separation, μs	1
Repetition frequency, Hz	10
Electron bunch length σ_z, cm	0.1
Normalized emittance, cm×rad	$\pi \times 10^{-3}$
Beta function at IP, cm	0.1
Diaphragm line	
Diaphragm separation, cm	100
Hole radius, cm	5
Power losses per one diaphragm	2×10^{-6}
Length, km	10
Optical system	
Laser power at CP, GW	300
Laser light wavelength, μm	1.06
Laser beam spot size at the mirror, cm	5
Focus distance of the mirror, cm	75
Conversion & Interaction regions	
Maximal energy of γ-quantums, GeV	206
Conversion efficiency $\eta_{e\gamma}$	0.7
Distance between CP and IP, cm	3
Luminosity $L_{\gamma\gamma}$, $\mathrm{cm^{-2}s^{-1}}$	1.5×10^{33}

2.1 Injection system

Since there is no need for positrons for the photon collider operation, the injection system could be simplified significantly. We assume that such a system can be constructed using a photoinjector technique. To provide the required parameters of the electron beam, it is sufficient to use the laser driven rf-gun with normalized brightness $B_\mathrm{n} \simeq 5 \times 10^7$ A $\mathrm{cm^{-2}rad^{-2}}$ ($B_\mathrm{n} = I/\epsilon_\mathrm{n}^2$, where I

is the beam current).

2.2 FEL amplifier

The source of the primary photons is the FEL amplifier designed by the MOPA (master oscillator - power amplifier) scheme. The radiation of the master oscillator (Nd:YLF laser, $\lambda = 1.053$ μm, peak power $W \simeq 100$ MW and average power ~ 10 W) is amplified in the FEL amplifier up to the power 350 GW. The master laser has parameters close to those used in the photoinjector laser systems [13].

Table 3
FEL amplifier parameters for the PLC

Electron beam	
Electron energy, GeV	10
Beam current, A	500
Energy spread, keV	500
Normalized emittance, cm×rad	$\pi \times 10^{-3}$
Undulator	
Undulator period, cm	40
Undulator field, kGs (enter./exit)	12 / 10.8
Length of untapered section, m	73
Total undulator length, m	330
Diaphragm line	
Diaphragm separation, cm	1
Hole radius, cm	0.3
Power losses per one diaphragm	1.1×10^{-5}
Radiation	
Radiation wavelength, μm	1.06
Input power, MW	100
Output power, GW	350
Efficiency, %	7

The main parameters of the FEL amplifier are presented in Table 3. The electron beam of the main accelerator ($\mathcal{E} = 10$ GeV, $I_{\rm peak} = 500$ A) is used as a driving beam. The undulator of the FEL amplifier is a helical one with

a period $\lambda_w = 40$ cm and a magnetic field at the axis $H_w \simeq 12$ kGs. It seems to be reasonable to construct the undulator using iron yokes and poles and water-cooled windings. Three dipoles, rotated by an angle of 120^0 with respect to each other, constitute a period of such an undulator (see Fig.3) [12]. The number of amper-turns should be equal to $NI \simeq 8000$ A$\times$turns for each winding at the pole gap of 1 cm. The main advantage of such a design is simplicity of manufacturing, the possibility of simple control of the undulator field, high reliability and relatively low cost.

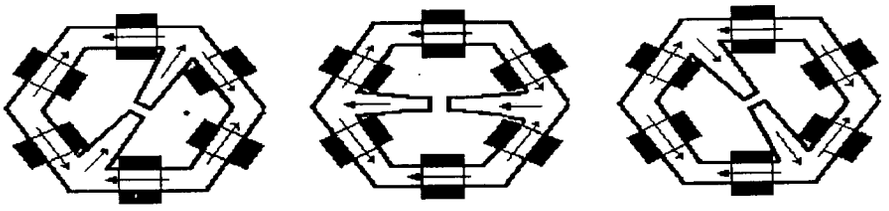

Fig. 3. Scheme of undulator design

An initial section of the undulator of 73 m length is untapered and provides exponential amplification of the radiation field of the master oscillator. To attain the required level of the output power, the final section of the undulator of 257 m length should be tapered. At the amplifier exit, the FEL efficiency is equal to 7 %.

Due to the relatively low value of the peak current, there is no possibility to use the conventional FEL amplifier scheme in which radiation is confined due to the "optical guiding" effect [9,10]. To overcome this problem, we use the scheme of the FEL amplifier with an open optical waveguide in the form of a diaphragm line [11].

2.3 Transporting channel for radiation

Having passed the FEL undulator, the electron beam is accelerated up to the final energy 250 GeV. Since the powerful optical bunch is produced at the very beginning of the accelerator, the next problem is to find a transport channel capable to transport the powerful radiation beam along a long distance without significant losses. This problem may be solved with a diaphragm focusing line which has the form of periodically spaced screens with round holes (see Appendix B). The diaphragm focusing line is placed in parallel to the main accelerator (see Fig.2). At large Fresnel number, the eigenmodes of such a waveguide have low diffraction losses. For instance, with a hole radius of 5 cm, a distance between the screens of 1 m and a radiation wavelength $\lambda \simeq 1$ μm, the relative radiation power losses per one diaphragm are of about 2×10^{-6} for the TEM_{00} ground mode. In the case under study, the total radiation power

losses along the transport channel are equal to 2%.

2.4 Conversion and interaction region

After passing their ways along the accelerator, electron and optical bunches should meet at the conversion point (see Fig.1). To provide optimal focusing conditions at the conversion point, the optical bunch should advance the electron bunch by several tens of centimeters. It is natural to use an optical delay line which provides the delay time equal to the time interval between bunches. In this case the radiation generated by one bunch is focused on the following one. The total radiation power losses in the diaphragm and the optical delay line are equal to 15 %. As a result, 300 GW of peak radiation power are transported to the conversion point. At optimal conditions of laser beam focusing on the electron beam (see Appendix A and Table 2), the conversion efficiency is about 0.7. Then high energy γ-quanta follow the initial electron trajectories and meet at the interaction point with the other γ-quantum beam produced by the opposite part of the collider. The integral luminosity of the colliding γ-beams is $L_{\gamma\gamma} \simeq 1.5 \times 10^{33}$ cm^{-2}s^{-1}.

3 Calculations of the FEL amplifier

In the case under study the "optical guiding" effect can not provide efficient confinement of the radiation which leads to a significant degradation of the FEL amplifier parameters. To solve this problem, we propose to use an FEL amplifier with a diaphragm line. Such an FEL amplifier scheme has been proposed in ref. [11] and can be used in FEL amplifier schemes for inertial confinement fusion. In this scheme a periodic diaphragm line is used for focusing and confinement of the radiation in the amplifier. It has the form of a sequence of totally absorbing screens with holes. At large values of the Fresnel number, the eigenmodes of the diaphragm line have rather small diffraction losses. At a relatively small gain of the radiation field amplitude along the undulator axis, the electron beam does not affect significantly the transverse distribution of the radiation field and the latter is defined mainly by the diaphragm line. The transverse field distribution of the TEM_{00} ground mode of the diaphragm line is of the form:

$$\mid \tilde{E} \mid \propto J_0(\nu_{01} r/R),$$

where r is transverse coordinate, R is the radius of the diaphragm line holes, J_0 is the Bessel function and ν_{01} is the first root of the Bessel function of zero

order. When the transverse size of the electron beam is much less than the aperture of the diaphragm line, the radiation field change across the electron beam can be neglected which reveals the possibility to use the one-dimensional approximation. In this case an "effective" beam current density can be substituted into the equations of the one-dimensional FEL amplifier theory:

$$j_0 = I\,[\,\pi R^2 J_1^2(\nu_{01})\,]^{-1} \simeq 3.7 I/(\pi R^2),$$

where I is the total beam current. In addition, the difference between the phase velocity of the TEM_{00} mode and the velocity of light c should be taken into account in the FEL resonance condition. In the case under study such an approach provides a correct description of the processes in the FEL amplifier with a diaphragm line. Thus, the calculation of the FEL amplifier can be performed in the framework of the one-dimensional model [14].

3.1 Working equations

Let us consider the electron beam moving along the z axis in the field of a helical undulator:

$$H_x + iH_y = H_w \exp\{-i\kappa_w z\}, \tag{1}$$

where $\kappa_w = 2\pi/\lambda_w$ is the undulator wavenumber. We neglect the transverse variation of the undulator magnetic field and assume that the electrons move along the constrained helical trajectories parallel to the z axis. The electron rotation angle θ_s is considered to be small and the longitudinal electron velocity v_z is close to the velocity of light c ($v_z \simeq c$).

The electric field of the amplified wave is presented in the complex form:

$$E_x + iE_y = \tilde{E}(x,y,z)\exp\,[\,i\omega(z/v_{ph} - t)\,]\,. \tag{2}$$

where ω is the frequency of the amplified wave and v_{ph} is the phase velocity of the TEM_{00} ground mode of the diaphragm line.

The equations of motion of the electron can be written in the form [14]:

$$\begin{aligned} d\mathcal{E}/dz &= u\cos(\psi + \psi_0), \\ d\psi/dz &= \kappa_w - \dot{\omega}(v_z^{-1} - v_{ph}^{-1}), \end{aligned} \tag{3}$$

where $v_z(\mathcal{E}, z)$ is the longitudinal velocity of the electron, u and ψ_0 are, respectively, the amplitude and the phase of the effective potential of the particle-wave interaction which are connected by the complex field amplitude $\tilde{E}(0,0,z)$ at the undulator axis as follows (we assume here $u > 0$):

$$(u/2)\exp(i\psi_0) = e^2 H_w \tilde{E}/2\kappa_w \mathcal{E}., \tag{4}$$

and $-e$ is the charge of the electron. Evolution of the amplitude and the phase of the effective potential is described by the following equations:

$$\begin{aligned} du/dz &= [\pi e^3 H_w^2/\kappa_w^2 \mathcal{E}^2 c]\, j_1 \cos(\psi_0 - \psi_1), \\ d\psi_0/dz &= -[\pi e^3 H_w^2/\kappa_w^2 \mathcal{E}^2 c]\,(j_1/u)\sin(\psi_0 - \psi_1), \end{aligned} \tag{5}$$

where j_1 and ψ_1 are, respectively, the amplitude and the phase of the first harmonic of the beam current density j_z:

$$\begin{aligned} j_1 \cos\psi_1 &= \frac{1}{\pi}\int_0^{2\pi} j_z \cos\psi d\psi, \\ j_1 \sin\psi_1 &= -\frac{1}{\pi}\int_0^{2\pi} j_z \sin\psi d\psi. \end{aligned} \tag{6}$$

Equations (3) and (5) constitute the self-consistent system of the one-dimensional model of the FEL amplifier.

At small deviations of the energy of the electrons from the nominal value $\mathcal{E}_0$, equations (3) and (5) can be simplified by using an expansion in the small parameter $P = (\mathcal{E} - \mathcal{E}_0)/\mathcal{E}_0$. It is convenient for the further considerations to use the reduced variables:

$$\hat{z} = \Lambda_0 z, \qquad \hat{C} = C/\Lambda_0, \qquad \hat{P} = \omega P/(c\gamma_z^2 \Lambda_0), \tag{7a}$$

$$\hat{u} = \omega u/c\gamma_z^2 \mathcal{E}_0 \Lambda_0^2, \qquad \hat{j}_1 = j_1/j_0. \tag{7b}$$

The detuning parameter C and the gain parameter Λ_0 are defined as

$$C = \kappa_w - \omega/2\gamma_z^2 c - \nu_{01}^2 c/2R^2\omega, \qquad \Lambda_0 = \left[\pi j_0 \theta_s^2 \omega/\gamma_z^2 \gamma I_A\right]^{1/3}, \tag{7c}$$

where $I_A = mc^3/e \simeq 17$ kA, $\gamma = \mathcal{E}_0/mc^2$, $\gamma_z^{-2} = \gamma^{-2} + \theta_s^2$, $\theta_s = Q/\gamma = eH_w/\kappa_w mc^2\gamma$ is the rotation angle of electron in the undulator and m is the mass of the electron. As a result, equations (3) and (5) take the form:

$$d\hat{P}/d\hat{z} = \hat{u}\cos(\psi + \psi_1),$$
$$d\psi/d\hat{z} = \hat{P} + \hat{C}, \tag{8}$$

$$d\hat{u}/d\hat{z} = \hat{j}_1 \cos(\psi_0 - \psi_1),$$
$$d\psi_0/d\hat{z} = -(\hat{j}_1/\hat{u})\sin(\psi_0 - \psi_1). \tag{9}$$

3.2 Numerical simulation algorithm

We simulate the electron beam with N macroparticles per interval $(0, 2\pi)$ over phase ψ. The beam current density $\hat{j}_z = j_z/j_0$ is calculated as

$$\hat{j}_z = -\frac{2\pi}{N}\sum_{j=1}^{N}\delta(\psi - \psi_{(j)}) \tag{10}$$

where $\psi_{(j)}$ are phases of the particles and $\delta(\psi - \psi_{(j)})$ is the delta function. It follows from eq. (10) that $\hat{j}_z$ has the following normalization:

$$\int_0^{2\pi} \hat{j}_z d\psi = -2\pi.$$

The amplitude $\hat{j}_1$ and phase ψ_1 of the first harmonic of the beam current density are given by the expressions:

$$\hat{j}_1 \cos\psi_1 = \frac{1}{\pi}\int_0^{2\pi} j_z \cos\psi d\psi = -\frac{2}{N}\sum_{j=1}^{N}\cos\psi_{(j)},$$
$$\hat{j}_1 \sin\psi_1 = -\frac{1}{\pi}\int_0^{2\pi} j_z \sin\psi d\psi = \frac{2}{N}\sum_{j=1}^{N}\sin\psi_{(j)}.$$

The equations of motion (8) for the N particles together with the field equations (9) compose the system of $2N + 2$ equations describing the amplification process in the FEL amplifier.

We consider the initial conditions when the electron beam is neither modulated in velocity nor in density and the amplitude of the TEM_{00} mode of the

electromagnetic wave at the undulator axis is equal to $E_{\rm ext}$. Then we have the following initial conditions at the undulator entrance at $z = 0$ ($j = 1, \ldots, N$):

$$\hat{P}_{(j)}(0) = 0, \qquad \hat{j}_1(0) = 0, \qquad \hat{u}(0) = \hat{u}_{\rm ext} = E_{\rm ext}/E_0,$$

where $E_0 = (c\gamma_z^2 \mathcal{E}_0 \Lambda_0^2)/(e\omega\theta_s)$.

3.3 Calculations of the FEL with untapered undulator

First, we consider the case that space charge fields and energy spread do not influence the FEL amplifier operation and that diffraction losses in the diaphragm line can be neglected.

In the linear high gain limit, when $\hat{u} \ll 1$ and $\hat{u}/\hat{u}_{\rm ext} \gg 1$, the field amplitude grows exponentially with the undulator length:

$$\hat{u}(\hat{z}) = \text{const} \times \exp(\mathrm{Re}\,\hat{\Lambda}\hat{z}), \tag{11}$$

where $\mathrm{Re}\,\hat{\Lambda}$ is the real part of the eigenvalue and in the case of exact resonance ($\hat{C} = 0$) is equal to:

$$\mathrm{Re}\,\hat{\Lambda} = \sqrt{3}/2. \tag{12}$$

The field stops growing in the saturation regime when the beam is overmodulated and a significant fraction of the electrons fall into the accelerating phase of the effective potential. The maximal value of the reduced field amplitude at $\hat{C} = 0$ is

$$\hat{u}_{\rm max} = \mid \tilde{E} \mid_{\rm max} / E_0 = 2.34. \tag{13}$$

The coordinate of the saturation can be found using the following relation ($\hat{z} = 0$ corresponds to the undulator entrance) [14]:

$$\hat{z}_{\rm max} = 3.1 + \frac{2}{\sqrt{3}} \ln(\hat{u}_{\rm ext}^{-1}). \tag{14}$$

In the high gain limit the FEL efficiency η can be defined as the ratio of the electromagnetic radiation power flux at the amplifier exit to the electron beam power flux at the undulator entrance. Taking into account eqs. (8) and (9) we can write:

$$\eta = ec \mid \hat{E}(0,0,z) \mid^2 \int_0^R 2\pi r J_0^2(\nu_{01} r/R) dr / 4\pi \mathcal{E}_0 I =$$

$$ec \mid \hat{E} \mid^2 / 4\pi \mathcal{E}_0 j_0 = \beta \hat{u}^2/4. \tag{15}$$

where

$$\beta = c\gamma_z^2 \Lambda_0/\omega. \tag{16}$$

The saturation parameter β is inversely proportional to the number of undulator periods and is always small. It is also useful to define the reduced efficiency $\hat{\eta} = \eta/\beta = \hat{u}^2/4$. At $\hat{C} = 0$ the maximal reduced FEL efficiency at saturation is

$$\hat{\eta}_{\rm sat} = \hat{u}^2_{\rm max}/4 = 1.37. \tag{17}$$

All the considerations presented above have been performed without taking into account the field attenuation in the diaphragm line. Such an approach is valid when the field attenuation is small at the gain length $l_g \simeq \Lambda_0^{-1}$. Using eq. (B.7), we obtain the following relation for the relative field decrease per one diaphragm:

$$K = 0.15(\lambda L)^{3/2}/R^3. \tag{18}$$

Thus, the losses in the focusing diaphragm line do not influence significantly the FEL amplifier operation when

$$K l_g/L \simeq 0.15\lambda^{3/2} L^{1/2}/\Lambda_0 R^3 \ll 1. \tag{19}$$

In order to calculate the parameters of the FEL amplifier we should define the value of the beam current I. Assuming the longitudinal distribution of the beam current to be Gaussian with $\sigma_z = 1$ mm, we find from Table 2 the peak value of the beam current, $I_{\rm max} \simeq 1$ kA. We will use the model of a homogeneous electron beam with a current $I = 0.5 \times I_{\rm max} \simeq 0.5$ kA and an effective length $2(2\pi)^{1/2}\sigma_z \simeq 5$ mm. We will prove below the validity of such a model. Substituting this value of the beam current into eqs. (7), (16) and (18), we obtain:

$$\Lambda_0 = 4.7 \times 10^{-4}\ {\rm cm}^{-1}, \quad K = 5.5 \times 10^{-6},$$
$$\beta = 1.5 \times 10^{-3}, \quad \hat{u}_{\rm ext} = 0.23. \tag{20}$$

We see, that the field attenuation in the diaphragm line is small and is about 1.2 % at the gain length and can be neglected. The FEL amplifier with untapered undulator saturates at $l_w = 103$ m and provides maximal efficiency $\eta_{sat} = 0.2$ % which is much less than the required value of 7 %.

3.4 Calculations of the FEL with tapered undulator

A reliable method to increase the FEL amplifier efficiency is the adiabatic change of the undulator parameters along the undulator axis (i.e. undulator tapering).

When the FEL efficiency increased significantly with respect to untapered case, but still remains small, $\hat{\eta} \ll 1$, the system of equations (8) and (9) can be used for calculations. The only distinction with the previous section is that in the case of undulator tapering the detuning

$$C = \kappa_w - \omega/2c\gamma_z^2 = \kappa_w - (1+Q^2)/2c\gamma^2, \tag{21}$$

depends on the longitudinal coordinate and is a function of the undulator period λ_w and undulator parameter Q . Here we consider a specific method of tapering, namely the change of the undulator field at fixed undulator period. The detuning is fixed at the initial section of the undulator and, starting from some distance $\hat{z}_i$, changes as a quadratic polynomial:

$$\hat{C}(\hat{z}) = k_0 + k_1(\hat{z} - \hat{z}_i) + k_2(\hat{z} - \hat{z}_i)^2. \tag{22}$$

The choice of the quadratic law of the tapering can be easily understood with a simple model situation. Let us consider the case of a completely bunched electron beam. It follows from the first equation of (9) that the field amplitude is growing proportionally to the undulator length. Then, it follows form the first equation of (8) that the change of the particle energy is proportional to the squared length of the undulator. Finally, from the second equation of system (8) we find, that the resonance condition takes place when the detuning parameter $\hat{C}$ is changed quadratically, too. This qualitative consideration allows one to find an asymptotic behaviour of the detuning $\hat{C}(\hat{z})$. So, in order to obtain optimal conditions of the tapering, the values of the four coefficients k_0, k_1, k_2 and $\hat{z}_i$ should be defined. We have performed a set of calculation to maximize the output amplitude at $(\hat{z} - \hat{z}_i) \gg 1$ and we obtained the following optimal values of the tapering parameters [14]:

$$k_0 = 0, \qquad k_1 = 1.44, \qquad k_2 = 0.36. \tag{23}$$

The optimal length of the untapered undulator section can be found from the relation:

$$\hat{z}_{\rm i} = 1.7 + \frac{2}{\sqrt{3}} \ln(\hat{u}_{\rm ext}^{-1}). \tag{24}$$

Comparison of relations (14) and (24) shows that the undulator tapering must start at a distance of $\Delta\hat{z} = 1.4$ before the saturation point of the untapered undulator. Phase analysis shows that at optimal parameters of the tapering (23), 65 % of the particles are trapped in the regime of coherent deceleration. The field amplitude at $(\hat{z} - \hat{z}_i) > 3$ can be calculated with the following approximate formula:

$$\hat{u} \simeq \hat{z} - \frac{2}{\sqrt{3}} \ln(\hat{u}_{\rm ext}^{-1}). \tag{25}$$

Using relations (14) and (24), we can calculate the total undulator length $\hat{z}_f$ of the FEL amplifier with efficiency $\hat{\eta}$:

$$\hat{z}_f \simeq 2\sqrt{\hat{\eta}} + \frac{2}{\sqrt{3}} \ln(\hat{u}_{\rm ext}^{-1}). \tag{26}$$

In the case under study the efficiency $\eta = 7$ % is achieved at the total undulator length 330 m ($\hat{z}_f \simeq 15.4$). The length of untapered section is equal to $z_{\rm i} \simeq 73$ m ($\hat{z}_{\rm i} = 3.4$).

In Fig.4 we present a plot of the dependence of the reduced field amplitude $\hat{u}(\hat{z})$ on the reduced undulator length. In this case $\hat{u}_{\rm ext} = 0.23$ which corresponds to a power of the $\rm TEM_{00}$ mode at the undulator entrance to be equal to $W_{\rm ext} = 100$ MW. Undulator tapering starts at $\hat{z}_{\rm i} = 3.4$ and detuning changes as

$$\hat{C} = 1.44(\hat{z} - 3.4) + 0.36(\hat{z} - 3.4)^2. \tag{27}$$

At the same figure we present the dependence of $\hat{u}(\hat{z})$ on $\hat{z}$ for untapered undulator. Fig.5 presents the phase distributions of the macroparticles at different coordinates of the tapered section.

It follows from the definition of the detuning C that in order to preserve the synchronism at the tapering with the fixed undulator period $\lambda_{\rm w}$, the undulator field $H_{\rm w}$ must be decreased as

$$\frac{H_{\rm w}(z_{\rm i}) - H_{\rm w}(z)}{H_{\rm w}(z_{\rm i}} = \alpha_1(z - z_{\rm i}) + \alpha_2(z - z_{\rm i})^2. \tag{28}$$

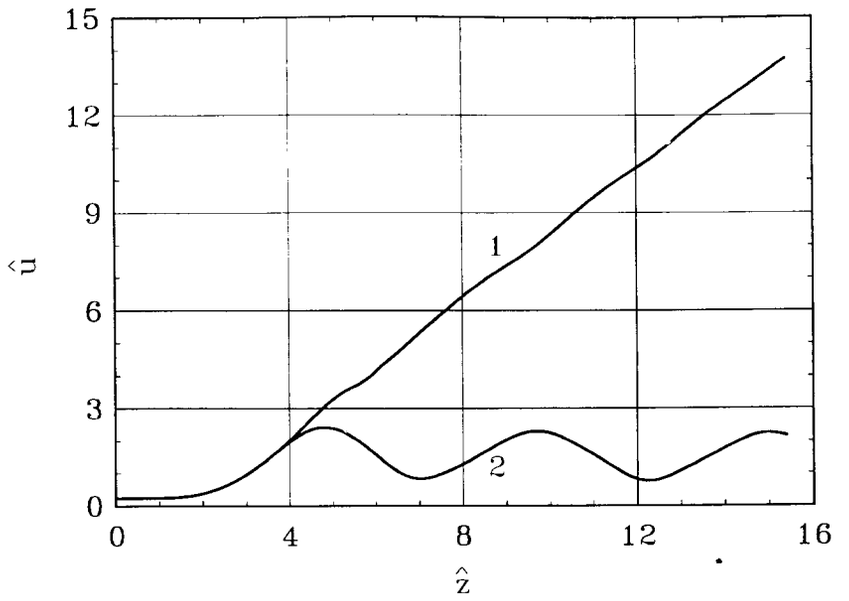

Fig. 4. Dependence of the reduced field amplitude versus the reduced undulator length. Curve (1) – untapered undulator, curve (2) – tapered undulator

The coefficients α_1 and α_2 are related to the coefficients k_1 and k_2 as:

$$k_1 = \frac{Q^2}{1+Q^2}\frac{\alpha_1}{\beta\Lambda_0}, \qquad k_2 = \frac{Q^2}{1+Q^2}\frac{\alpha_2}{\beta\Lambda_0^2}, \tag{29}$$

Using relations (27) – (29) we find that the undulator field amplitude at the undulator exit is $H_w(z_f) = 10.8$ kGs .

3.5 Validity of low efficiency approximation

The simulations of the nonlinear regime of the FEL amplifier operation presented above, have been performed with equations (8) and (9) which has been derived from the initial equations (3) and (5) by an expansion in the small parameter $P = (\mathcal{E} - \mathcal{E}_0)/\mathcal{E}_0$. While this approach is valid in the low efficiency case, its validity should be carefully checked in the case under study when the final FEL efficiency is of about 7 %.

We normalize eqs. (3) and (5) in the same manner as was done in section 3.2 with the only refinement that all the normalization factors, Q and $\beta = \gamma_z^2\Lambda_0/\omega$, are calculated using the initial values of the beam and undulator parameters:

(a)

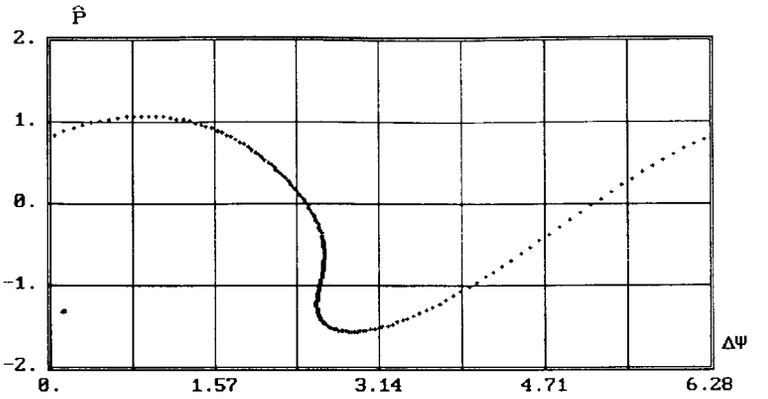

(b)

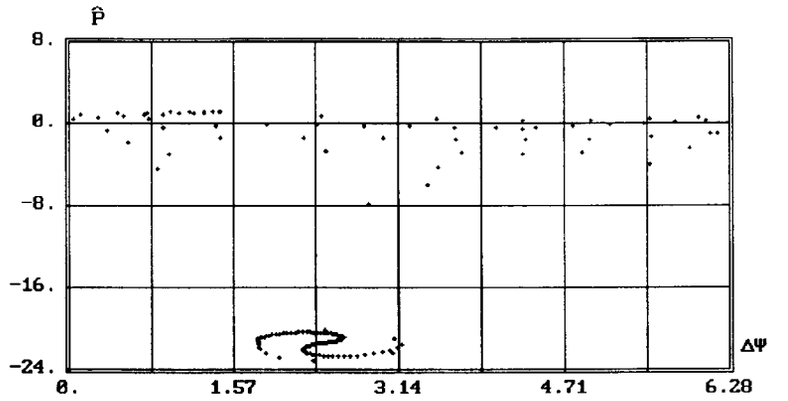

(c)

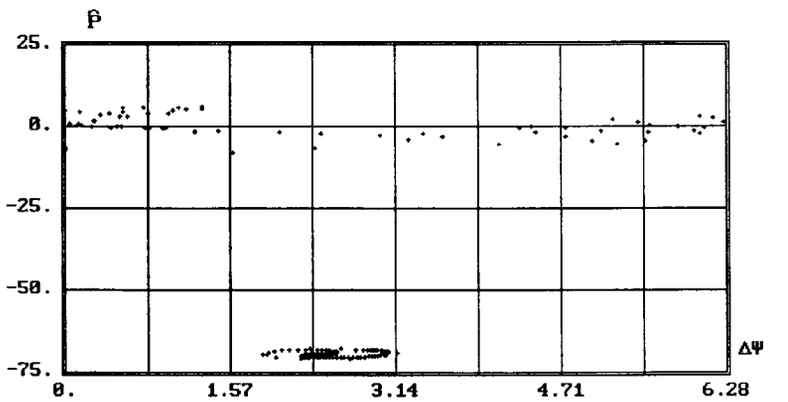

Fig. 5. Phase space distribution of the particles in the case of the undulator tapering according to the law $\hat{C} = 0$ at $\hat{z} < 3.4$ and $\hat{C} = 1.44 \times (\hat{z} - 3.4) + 0.36 \times (\hat{z} - 3.4)^2$ at $\hat{z} > 3.4$. (a): $\hat{z} = 3.4$, (b): $\hat{z} = 9.4$ and (c): $\hat{z} = 15.4$. Here $\hat{\Lambda}_{\rm p}^2 = 0$, $\hat{\Lambda}_{\rm T}^2 = 0$ and $\hat{u}_{\rm ext} = 0.23$.

$$\frac{d\hat{P}}{d\hat{z}} = \frac{1}{(1+3\hat{P})}\left(1 - \frac{1+Q^2}{Q^2}\beta T(\hat{z})\right)\hat{u}\cos(\psi+\psi_0),$$

$$\frac{d\psi}{d\hat{z}} = \frac{1}{(1+3\hat{P})^2}\left\{\hat{P}\left(1+\frac{\beta\hat{P}}{2}\right) + T(\hat{z})\left(1 - \frac{1+Q^2}{2Q^2}\beta T(\hat{z})\right)\right\}, \qquad (30)$$

$$\frac{d\hat{u}}{d\hat{z}} = -\left(1 - \frac{1+Q^2}{Q^2}\beta T(\hat{z})\right)\frac{2}{N}\sum_{j=1}^{N}\frac{\cos(\psi_{(j)}+\psi_0)}{1+\beta\hat{P}_j},$$

$$\frac{d\psi_0}{d\hat{z}} = \frac{1}{\hat{u}}\left(1 - \frac{1+Q^2}{Q^2}\beta T(\hat{z})\right)\frac{2}{N}\sum_{j=1}^{N}\frac{\sin(\psi_{(j)}+\psi_0)}{1+\beta\hat{P}_j}. \qquad (31)$$

Taking into account expression (28), the function $T(\hat{z})$ is written in the form:

$$T(\hat{z}) = k_0 + k_1(\hat{z} - \hat{z}_i) + k_2(\hat{z} - \hat{z}_i)^2, \qquad (32)$$

where coefficients k_j and α_j are connected with eqs. (29).

At a sufficiently short undulator length the energy losses of the trapped particle are small, $\Delta\mathcal{E}/\mathcal{E}_0 = \beta\hat{P} \ll 1$ and the system of equations (30) and (31) reduces to the system of equations (8) and (9). In this case the detuning parameter $\hat{C}(\hat{z})$ is equal to $T(\hat{z})$ and the growing of the field amplitude $\hat{u}(z,\beta)$ is the same as for $\hat{u}(\hat{z})$ (see Fig.4). In this initial section the average energy of the trapped particles decreases quadratically with the undulator length, compensating for the quadratic increase of the parameter $T(\hat{z})$ in the equation $d\upsilon/d\hat{z} = \hat{P} + T(\hat{z})$ of the system (30). The average change of the phase of the trapped particles is zero, $< d\psi/d\hat{z} >= 0$, and their motion corresponds to phase oscillations about the equilibrium decelerating phase $\psi_e + \psi_0 = \text{const}$ (according to the second equation of the system (31), at $\hat{u} \gg 1$ the change of the phase of the effective potential ψ_0 can be neglected). As the length of the undulator is increased, the difference between the approximate system of equations (8) and (9) and the original system (30) and (31) begins to become significant and in the general case the latter system should be used for simulations.

A thorough analysis presented in ref. [14] has shown that simulations based on the low efficiency approximation are valid in two cases. First, they are valid at a large value of the undulator parameter $Q \gg 1$ and can even be used when the FEL efficiency is close to unity. Secondly, in the case when Q is of the order of unity and the saturation parameter $\beta < 0.3$, the low efficiency approximation provides sufficient accuracy of the calculations when the FEL efficiency is less than 10 %. In the case under study we have $Q = 45$ and $\eta = 7$ %, so this FEL amplifier can be calculated using the low efficiency approximation.

3.6 Noise of the FEL amplifier

The power of the master oscillator $W_{\rm ext}$ should be much higher than the intrinsic noise of the FEL amplifier $< W_{sh} >$. Let us estimate the value of the FEL amplifier noise. Assuming that the number of electrons emitted from the cathode fluctuates randomly in time, we can write the expression for the rms value of the beam current fluctuations in the frequency band $\Delta\omega$:

$$< (\Delta I)^2 > \simeq eI\Delta\omega/\pi. \tag{33}$$

Then we should remember that the frequency bandwidth of the FEL amplifier operating in a linear regime is

$$\Delta\omega/\omega_0 \simeq \Lambda_0/\kappa_{\rm w}. \tag{34}$$

These fluctuations of the beam current (or, in other words, the fluctuations of the beam density) play the role of an external signal. The "effective power" of such a signal can be estimated as the value of the radiation power emitted by the electron beam with initial modulation given by eq. (33) at one gain length Λ_0^{-1}:

$$< W_{sh} > \simeq < (\Delta I)^2 > \theta_{\rm s}^2/c\Lambda_0^2 R^2. \tag{35}$$

Taking into account eqs. (33) and (34) we finally obtain:

$$< W_{sh} > \simeq eI\theta_{\rm s}^2\gamma_{\rm z}^2/\Lambda_0 R^2. \tag{36}$$

Here we should emphasize that the effective power of the shot noise in the FEL amplifier with diaphragm line is defined by the value of the total beam current. This is connected with the fact that in such an FEL the transverse size of the optical beam is defined by the focusing diaphragm line and is much wider than the transverse size of the electron beam. As a result, the process of the amplification is defined by the value of the total beam current.

In the case under consideration (see Table 3), the effective power of the shot noise is about 1 W.

3.7 Axial nonuniformity of the beam current

In the considerations presented above we have approximated the axial distribution of the beam current by a flat-top pulse of 500 A and $2\sqrt{2\pi}\sigma_{\rm z} \simeq 5$ mm

length. In the real situation the beam current has a Gaussian distribution with peak current equal to 1 kA and half-width $\sigma_z = 1$ mm. We should prove the validity of such a model. It was shown in ref. [14] that the efficiency of the FEL amplifier with the tapered undulator does not vary significantly when the beam current increases significantly with respect to nominal value and the output power grows proportionally to the beam current. On the other hand, the FEL efficiency (and the output power) is decreased rapidly with the beam current decrease. It is explained by the peculiar features of the regime of coherent deceleration. In particular, the optimal value of the tapering coefficient k_2 is 0.36. The regime of coherent deceleration remains stable when k_2 is decreased and becomes unstable in the opposite case. Remembering that k_2 is inversely proportional to the beam current I, we can understand such a dependency of the FEL amplifier efficiency on the beam current. So, in order to provide effective conditions for the FEL operation, its optimization should be performed not at the peak value of the beam current, but at a smaller value of the beam current. Fig.6 presents the actual axial distribution of the beam current and the corresponding distribution of the output power of the FEL amplifier with optimized parameters. Using these plots we find that the integrated energy in one pulse is about 5.7 J within the "effective" pulse duration 17 ps which corresponds to the average power 350 GW, just the same value which is produced by the model electron bunch.

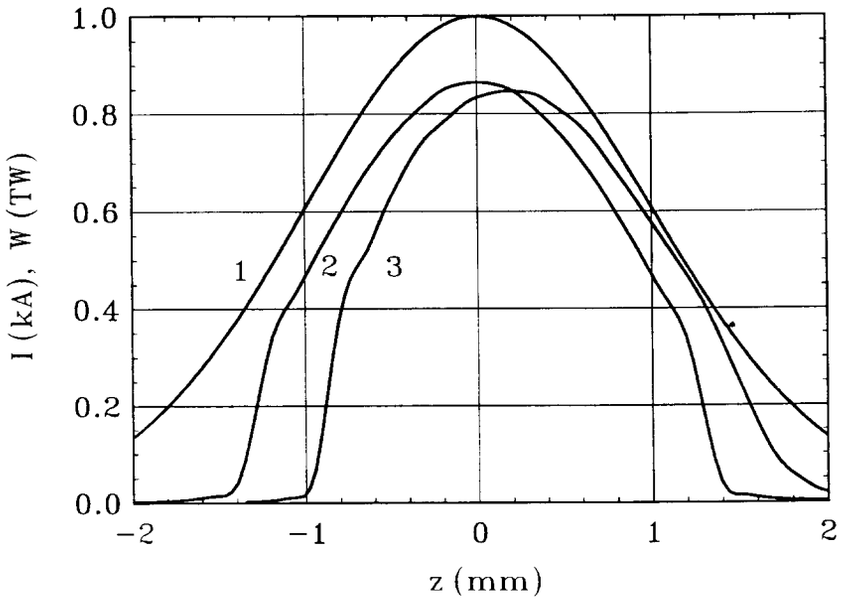

Fig. 6. Axial distribution of the beam current in the elctron beam (curve 1) and axial distribution of the output power in the optical beam (curves 2 and 3). Curve 2 (3) are calculated without (with) taking into account the slippage effect.

3.8 Slippage effects

In the calculations performed until now we neglected the slippage effects. The curve 3 in Fig.6 presents the results of more accurate calculations taking into account slippage effects and axial distribution of the beam current. Comparing this curve with curve 2 at the same figure, we conclude that slippage effects do not influence significantly the FEL amplifier operation.

3.9 Energy spread and emittance effects

The energy spread of the beam has been included in the simulation algorithm by dividing all the macroparticles in the phase interval $0 \leq \psi \leq 2\pi$ for $\hat{z} = 0$ into a small even number N_ψ of groups. The macroparticles in each group have identical phases ψ for $\hat{z} = 0$. The initial values of the reduced momenta $\hat{P}_j$ of the particles in each group ($i = 1, \ldots, N_\mathrm{p}$) are described by a Gaussian distribution

$$F(\hat{P}) = (2\pi\hat{\Lambda}_\mathrm{T}^2)^{-1/2} \exp[-\hat{P}^2/(2\hat{\Lambda}_\mathrm{T}^2)] \tag{37}$$

with rms deviation $< (\Delta\hat{P})^2 >= \hat{\Lambda}_\mathrm{T}^2$. The phases of the groups of particles for $\hat{z} = 0$ were distributed in the interval from 0 to 2π in such a way that the amplitude of the first harmonic of the macroparticle density was equal to zero.

Using equations (30) and (31) we have studied the influence of the energy spread on the trapping efficiency of the FEL amplifier. When performing optimization, we changed the detuning by the following law:

$$\hat{C} = \begin{cases} \hat{C}_\mathrm{m} & \text{at } \hat{z} < \hat{z}_\mathrm{i}, \\ \hat{C} = \hat{C}_\mathrm{m} + k_1(\hat{z} - \hat{z}_\mathrm{i}) + k_2(\hat{z} - \hat{z}_\mathrm{i})^2 & \text{at } \hat{z} > \hat{z}_\mathrm{i}, \end{cases} \tag{38}$$

where $\hat{C}_\mathrm{m}$ is the detuning corresponding to the maximal value of the increment in the linear mode of operation. The optimization procedure consisted in finding optimal values of the tapering coefficients k_1, k_2 and $\hat{z}_\mathrm{i}$ (as functions of the energy spread) to maximize the field amplitude at $\hat{z} - \hat{z}_\mathrm{i} \gg 1$. Fig.7 illustrates the dependence of the trapping factor as a function of the space charge parameter.

Assuming the energy spread in the beam to be Gaussian with the rms dispersion $\sigma/\mathcal{E}_0 \simeq 0.005$ % (see Table 3), we calculate the energy spread parameter

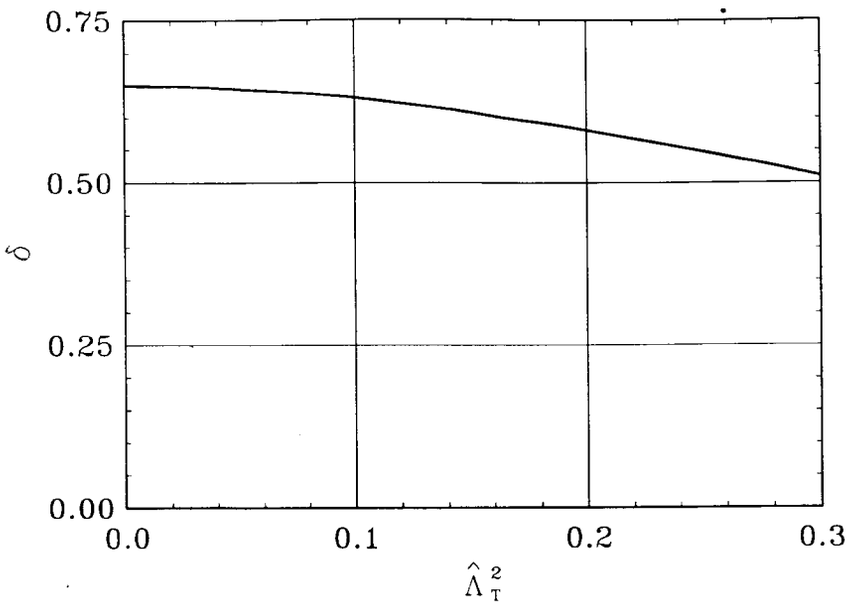

Fig. 7. Dependence of the trapping factor on the energy spread parameter.

$\hat{\Lambda}_T^2$ appearing in eq. (37):

$$\hat{\Lambda}_T^2 = \sigma^2/\beta^2\mathcal{E}_0^2 \simeq 0.001. \tag{39}$$

It is seen from the plot in Fig.7 that such a value of the energy spread does not influence the FEL amplifier operation.

The finite value of the electron beam emittance results in the angular spread of the electrons in the beam and in an additional spread of the longitudinal electron velocities. The emittance effects can be taken into account as follows. As a rule, the electron beam should be matched with the focusing system of the undulator which results in the following values of the beam radius r_0 and angle spread $(<(\Delta\theta)^2>)^{1/2}$ in the beam:

$$r_0 = (\beta_w \epsilon_n/\pi)^{1/2}, \qquad (<(\Delta\theta)^2>)^{1/2} = (\epsilon_n/\pi\beta_w\gamma)^{1/2} \tag{40}$$

where $\beta_w = \sqrt{2}\,\lambda_w/2\pi\theta_w$ is the beta-function of the electron beam in the undulator and ϵ_n is the normalized emittance of the beam. The presence of the angle spread in the beam results in an additional spread in the longitudinal velocities which may be interpreted as an additional energy spread. So, the inclusion of the emittance effects is performed by substituting the real energy spread $\sigma_E = [<(\Delta\mathcal{E}/\mathcal{E})^2>]^{1/2}$ in the energy spread parameter by "effective" energy spread

$$\sigma_E = [<(\Delta\mathcal{E}/\mathcal{E})^2> + \gamma_z^4 <(\Delta\theta)^2>^2 /4]^{1/2}.$$

Using the parameters presented in Table 3 we obtain the following value of the "effective" energy spread due to emittance:

$$(\hat{\Lambda}_T^2)_{\text{eff}} \simeq \gamma_z^4 (< (\Delta\theta)^2 >)^2 / 4\beta^2 \simeq 10^{-6}. \tag{41}$$

and its contribution to the longitudinal velocity spread is negligibly small.

3.10 Restrictions on the energy deviation

Fig.8 presents the dependency of the FEL amplifier output power on the reduced detuning $\hat{C}$. This plot enables one to find restrictions on the values of systematical drifts: frequency of the master oscillator $\Delta\omega/\omega = 2\beta \cdot \Delta\hat{C}$; energy deviation $\Delta\mathcal{E}/\mathcal{E} = \beta \cdot \Delta\hat{C}$; undulator field $\Delta H_w/H_w = \beta(1+Q^2) \cdot \Delta\hat{C}/Q^2$ (here the reduced bandwidth of the amplifier $\Delta\hat{C}$ is determined by the requirements on the stability of the output power level). It is seen from the plot in Fig.8 that systematical drifts $\sim$ 0.1 % of the above mentioned parameters do not influence significantly the FEL amplifier output power.

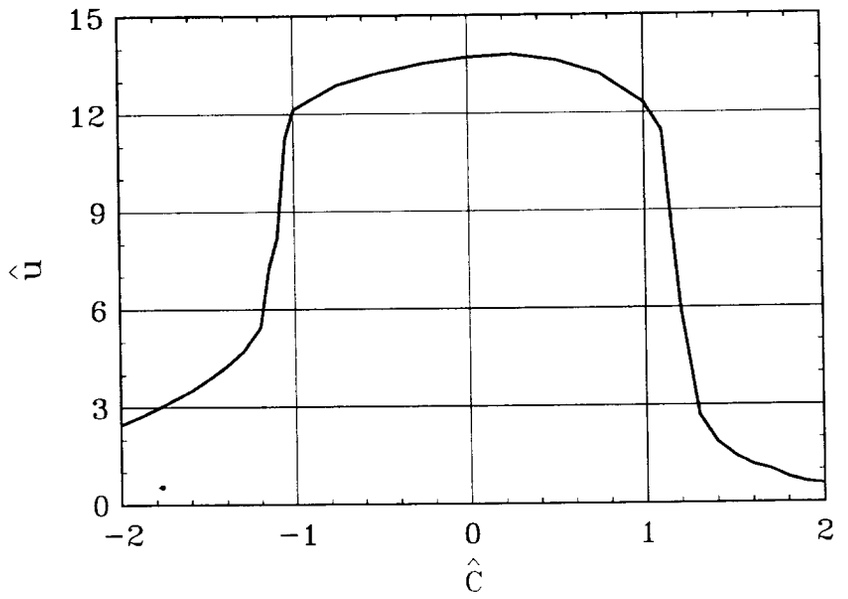

Fig. 8. Dependence of the output field amplitude at the amplifier exit on the detuning parameter.

It should be noticed that the electron beam, produced by the RF accelerator, has finite phase extent with respect to the accelerating RF wavelength. It results in a drift of the mean energy of the particles along the beam. Using Table 1, one can obtain that the half-width of this distribution is equal to $\delta\mathcal{E}/\mathcal{E}_0 \simeq (1/4)(\pi\sigma_z/\lambda_{\text{rf}})^2 \simeq 0.02$ %. In accordance with the plot presented in Fig.8, such value of energy drift does not influence on the FEL output power.

3.11 Influence of synchrotron radiation on the FEL amplifier operation

When electrons move in the undulator of the FEL amplifier they radiate incoherent synchrotron radiation, too. This results in the decrease of the mean energy and increase of the energy spread in the electron beam due to the quantum fluctuations of synchrotron radiation.

Energy losses of electron due to synchrotron radiation are given with the expression:

$$d\mathcal{E}_0/dz = 2r_e^2\gamma^2 H_{\rm w}^2(z)/3,$$

where $r_e = e^2/mc^2$.

In the present example the total energy losses in the undulator are about $\Delta\mathcal{E}_{\rm sr}/\mathcal{E}_0 \simeq 0.5$ %. These energy losses do not interfere with the FEL amplifier operation, because they may be compensated by an appropriate tuning of the magnetic field of the undulator, thus providing the resonance condition.

A more harmful influence of synchrotron radiation may be caused by the growth of the energy spread in the electron beam due to the quantum fluctuations of synchrotron radiation. The rate of the energy diffusion is given by the expression:

$$< d(\delta\mathcal{E})^2/dz >= 55e\hbar\gamma^4 r_e^2 H_{\rm w}^3/24\sqrt{3}mc.$$

The resulting energy spread is given by the expression:

$$(\Delta\mathcal{E})_{\rm fl} \simeq [(\Delta\mathcal{E})_{\rm sr}\hbar\omega_{\rm sr}]^{1/2},$$

where $(\Delta\mathcal{E})_{\rm sr}$ are the total energy losses of the electron due to the synchrotron radiation and $\hbar\omega_{\rm sr} = 3e\hbar\gamma^2 H_{\rm w}/2mc$ is the characteristic energy of the synchrotron radiation γ-quanta. In the present example the increase in the energy spread is about $(\Delta\mathcal{E})_{\rm fl}/\mathcal{E}_0 \simeq 0.02$ %. Numerical simulations have shown that such an energy spread does not decrease significantly the FEL amplifier efficiency.

3.12 Applicability region of the single-mode approximation

A peculiar feature of the FEL amplifier calculations presented above is the use of the single-mode approximation. Namely, we assume that the amplified wave corresponds to the TEM_{00} ground mode of the empty waveguide. On the other hand, in the general case the eigenmode of an active waveguide is the superposition of modes of the empty waveguide. With respect to this a reasonable question arises on the validity region of such an approximation.

In Appendix C we present rigorous results of the linear theory of the FEL amplifier with a diaphragm focusing line. In the linear high gain limit the radiation of the electron beam in the undulator can be represented as a set of modes. When amplification takes place, the mode configuration in the transverse plane remains unchanged while the amplitude grows exponentially with the undulator length. Each mode is characterized by the increment eigenvalue and the field distribution eigenfunction in terms of transverse coordinates. In the general case the eigenmode of an active waveguide is a superposition of modes of the empty waveguide. The mode with the highest increment is dominating all other modes. Following the gain process along the undulator axis one finds that the field distribution is settled corresponding to the mode with the maximum increment.

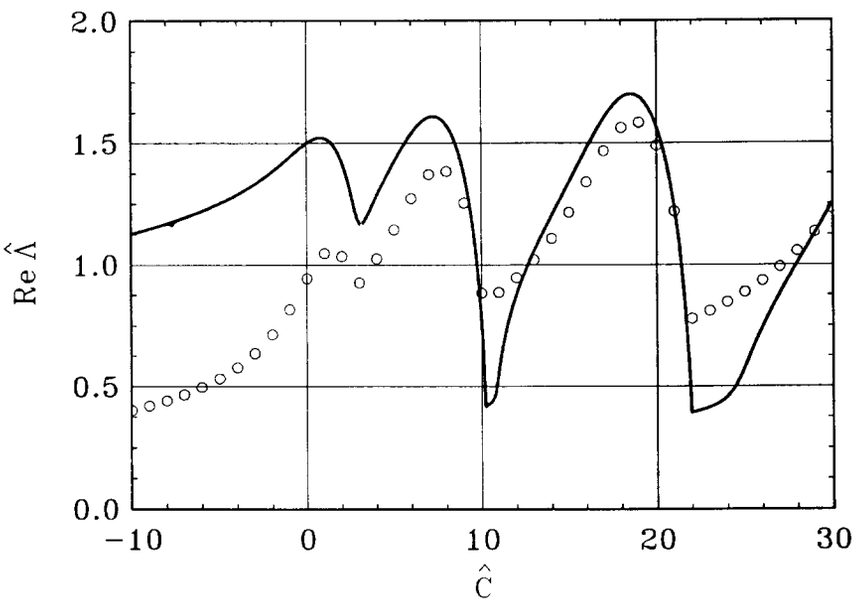

Fig. 9. Dependence of the reduced increment on the detuning. The parameters of the numerical example correspond to the parameters of the FEL amplifier from Table 3. The solid curve is the result of a solution of the exact eigenvalue equation (C.17) and the circles correspond to the one-dimensional approximation (C.32).

In Fig.9 we present the dependency of the maximal increment on the detuning for axisymmetric modes. It is seen that this dependence has a character

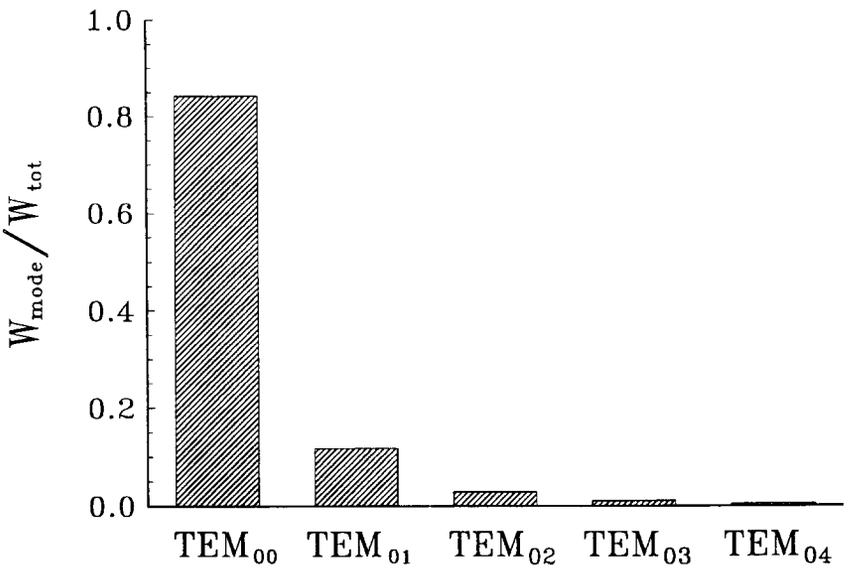

Fig. 10. Relative contribution of the modes of the empty waveguide into the power of the beam radiation mode. Parameters of the numerical example correspond to the parameters of the FEL amplifier from Table 3. Here $\hat{C} = 0.8$ (see Fig.9).

of maxima series. The physical nature of this phenomenon is illustrated with the plots presented in Fig.10 where histogram of the relative contributions of the passive waveguide modes into the power of the beam radiation mode, are presented. One can find from these plots that each time when the resonant condition of the beam with the corresponding passive waveguide mode is fulfilled, the contribution of the latter to the beam radiation mode becomes dominating. This case is rather well described by a single-mode approximation and in the first maximum the eigenmode of the active waveguide is described rather well with the TEM_{00} ground mode of the empty waveguide, of about $\simeq$ 80 % of total power corresponds to the contribution of this mode.

So, we see that with the given parameters of the FEL amplifier (see Table 3), the calculations of the linear regime could be performed using the single-mode approximation. It is evident that this approximation is applicable for a calculation of the nonlinear regime of the FEL amplifier operation, too, because in this case the rate of the field growth is much less than in the linear regime and the field eigenmode is more close to the TEM_{00} ground mode of the empty waveguide.

4 Test facility

The basic idea of the proposal, namely the possibility to construct the FEL amplifier with a diaphragm focusing line, requires experimental verification.

To perform such a verification, there is no need to build a full-scale facility. It may be done at a scaled model of the FEL amplifier with parameters presented in Table 4.

Table 4
Parameters of the FEL at the Tesla Test Facility

Electron beam	
Electron energy, GeV	0.5
Beam current, A	500
Energy spread, keV	500
Normalized emittance, cm×rad	$\pi \times 10^{-3}$
Undulator	
Undulator period, cm	20
Undulator field, kGs (enter./exit)	5.4 / 4.8
Length of untapered section, m	9
Total undulator length, m	20
Diaphragm line	
Diaphragm separation, cm	1
Hole radius, cm	0.3
Power losses per one diaphragm	3.4×10^{-4}
Radiation	
Radiation wavelength, μm	10.6
Input power. MW	10
Output power, GW	17.5
Efficiency, %	7

The parameters of the electron beam correspond to the parameters of the electron beam from the accelerator which will be constructed at the TESLA Test Facility at DESY [17]. It is assumed that the time diagram of the TESLA Test Facility operation will correspond to that of the main TESLA project. According to formulae (7) and (16), we obtain the following parameters of the test FEL:

$$\Lambda_0 = 4.3 \times 10^{-3}\mathrm{cm}^{-1}, \qquad K = 1.7 \times 10^{-4},$$
$$\beta = 6.9 \times 10^{-3}, \qquad \hat{u}_{\mathrm{ext}} = 0.15. \tag{42}$$

The field attenuation in the diaphragm line is of about 3.6 % at the gain length and is negligibly small with respect to the field gain at the same length. Saturation efficiency and saturation length of the amplifier are $\eta_{\rm sat} = 0.9$ % and $l_{\rm w} = 12$ m, respectively. When the undulator is tapered according to eqs. (28), (23) and (29), it will provide the efficiency $\eta = 7$ % at the total undulator length equal to 20 m ($\hat{z}_f = 8.6$). The length of untapered section is equal to $z_{\rm i} \simeq 9$ m ($\hat{z}_{\rm i} = 3.9$).

The test FEL amplifier will play the role of a scaled model of the FEL amplifier for the photon linear collider. The parameters of the test FEL are chosen in such a way that from the physical point of view the process of amplification is identical to that of the full-scale FEL amplifier. In particular, in order to provide such a scaling, the operating wavelength of the test FEL is chosen to be equal to 10 μm. Using the formulae presented in section 3 and Appendix C, one finds that the values of the reduced variables for the test and full-scale FEL are close to each other. The field eigenmode of the test FEL is close to that of the full-scale amplifier, too.

5 Discussion

In the present paper we have shown that application of the FEL technique reveals a possibility to construct a photon linear collider at TESLA. We have studied in detail the most economical FEL scheme where the electron beam of the main accelerator serves as a driving beam for the FEL amplifier. Such an approach naturally provides synchronization of the optical and the laser bunches and the generation of the laser beam with the required pulse duration and repetition rate.

In order to make the FEL amplifier operation more effective, we have proposed to use the FEL amplifier with a diaphragm focusing line. In order to transport the powerful laser radiation to the conversion point it was proposed to use an open waveguide in the form of a diaphragm line wherein focusing of radiation is provided due to diffraction effects.

It was shown that the TESLA Test Facility can be used for a construction of a scaled model of the FEL for future full-scale photon collider at the TESLA.

In the present paper we have limited our consideration to the study of the specific photon collider scheme aiming to show the feasibility of the PLC construction. There is a wide region for modification of this scheme. For instance, taking into account the peculiar feature of the TESLA project, namely, multi-bunch mode operation, a scheme with only one free electron laser can be used. It operates as follows. The FEL is installed only in one branch of the linear

collider. When the laser bunch passes the focus of the conversion region, it is not dumped but is directed to the optical delay line which provides a delay time equal to the time interval between the bunches (1 μs). Then it is focused on the electron beam of the opposite branch of the linear collider. Of course, this configuration provides colliding gamma-beams with the second micropulse of the collider. Nevertheless, the number of microbunches is 800, so it will not result in significant reduction of the integral luminosity. There may be also an approach where the driving beam for the FEL is produced by a separate linear accelerator.

In conclusion we should note that there is a significant problem in the e^+e^- version of the TESLA project, namely that of positron production which is not resolved till now. From this point of view it seems to be more feasible to begin the TESLA construction with the $\gamma\gamma$ version. From a technical point of view the construction of the photon linear collider seems to be more simple. First, there is no need for positrons for the PLC operation, so the injection system of the collider can be simplified significantly. For instance, there is no need for a damping ring and a flat electron beam and the injection system could be built on the base of the photoinjector technique. The installation of the free electron laser system ($\lambda = 1.053$ μm, $W_{\rm peak} \simeq 300$ GW) will enable to achieve luminosity up to $L_{\gamma\gamma} \simeq 1.5 \times 10^{33}$ cm^{-2}s^{-1}.

Acknowledgements

The authors express great gratitude to Dr. R. Settles and Dr. H. Mais for reading our manuscript and useful recommendations. We are also grateful to Prof. B.H. Wiik, Prof. A. Wagner, Dr. M. Leenen and Dr. J. Rossbach for their interest in our work.

A Obtaining colliding $\gamma\gamma$ beams

The most optimal way to produce high energy γ - quanta is the Compton backscattering of the laser photons by the high energy electrons [5]. The frequencies of the incident and scattered photons, ω and ω_γ, are connected by the relation (in the small-angle approximation):

$$\hbar\omega_\gamma = \frac{\mathcal{E}\chi}{1+\chi+\gamma^2\theta^2}, \tag{A.1}$$

where θ is the scattering angle, $\chi = 4\gamma\hbar\omega/m_e c^2$, m_e and $\mathcal{E}$ are the electron mass and energy, respectively, and $\gamma = \mathcal{E}/m_e c^2$ is relativistic factor.

Focusing of laser beam

To obtain an effective conversion of the primary laser photons into the high energy photons, the laser beam should be focused on the electron beam. It may be performed, for instance, by means of a metal focusing mirror (see Fig.1). Electrons move along the z axis and pass through the mirror focus. To calculate the conversion coefficient, it is necessary to find the distribution of the optical field intensity in the focal spot. We assume the focus distance and aperture of the focusing mirror to be F and a, respectively. All the calculations will be performed using paraxial approximation, i.e. it means that the angle of incident laser beam α with respect to the mirror normal and $\theta_{\max} \simeq a/F$ are much less than unity.

First we consider the case of infinitely long laser pulse. To be concrete, we assume the laser radiation to be circularly polarized. Electric field of the laser electromagnetic wave is presented in the following complex form:

$$E_x + iE_y = \tilde{E}(x,y,z)\exp[i\omega(z/c-t)].$$

In axisymmetric case, the expression for the optical field distribution on the mirror surface may be written in the form:

$$\tilde{E}(x,y,z)|_{z=F} \simeq \tilde{E}_0(r),$$

where $r = (x^2+y^2)^{1/2}$ (it is assumed that the coordinate system origin is placed in the geometrical focus of the mirror). Thus, using Huygens-Fresnel

integral, one can find distribution of the optical field in the focus vicinity [20]:

$$E = |\tilde{E}(z,r)| = \frac{\omega}{cF}\Big|\int_0^a \tilde{E}_0(\rho)J_0(v\rho)\exp(-iu\rho^2)\rho d\rho\Big|, \tag{A.2}$$

where $v = \omega r/cF$ and $u = \omega z/2cF^2$. Let us perform physical analysis of this expression. When the optical field intensity on the mirror surface is uniform one:

$$\tilde{E}_0(r) = A = const \qquad \text{at} \qquad 0 < r < a, \tag{A.3}$$

then intensity distribution in the focal plane $I(0,r)$ is given with the expression:

$$I(0,r) = |\tilde{E}(0,r)|^2/4\pi c = I_0\left[\frac{2J_1(v_a r)}{v_a r}\right]^2, \tag{A.4}$$

where $I_0 = A^2\omega a^2/2$ is the optical field intensity in the geometrical focal point and $v_a = \omega a/cF$. It is seen from expression (A.4) that the optical field intensity takes the first zero value at $v_a r = 3.88$, i.e at

$$r = 3.88cF/\omega a. \tag{A.5}$$

and more than 80% of the total optical power is passed inside the first diffraction maximum.

The distribution of the optical field intensity along z axis is given with expression:

$$I(z,0) = I_0[2\sin(ua^2/2)/ua^2]^2. \tag{A.6}$$

The optical field intensity takes its first zero value at the distance

$$z = \pm 4\pi cF^2/\omega a^2 \tag{A.7}$$

from the geometrical focus of the mirror. So, simple physical estimations show that characteristic dimensions of the region with strong optical field are od the order of:

$$r \lesssim 4cF/\omega a. \qquad |z| \lesssim 4\pi cF^2/\omega a^2. \tag{A.8}$$

When calculating the conversion efficiency, we assume transverse electron beam size at the conversion point σ_F to be small with respect to the laser beam spot size :

$$\sigma_F^2 \ll (4cF/\omega a_0)^2. \tag{A.9}$$

where a_0 is the characteristic size of laser beam on the focusing mirror. So, when calculating the probability of the Compton scattering, it is sufficient to take into account the variation of the optical field amplitude along the z axis only. When the electron transverse motion in the field of incident electromagnetic wave is nonrelativistic:

$$\frac{e^2}{m_e^2 c^4}|\tilde{E}|^2 \lambda\!\!\!^{-2} \ll 1, \tag{A.10}$$

the probability P of the electron scattering by the incident optical beam is given with the expression [4]:

$$P = 1 - \exp[-(2\sigma_c/4\pi\hbar\omega) \int_{-\infty}^{\infty} |\tilde{E}(z,0)|^2 dz], \tag{A.11}$$

where

$$\sigma_c = 2\pi r_e^2 [\frac{1}{\chi}\ln(1+\chi) - \frac{8+4\chi}{\chi^3}\ln(1+\chi) + \frac{8}{\chi^2} + \frac{2+\chi}{2(1+\chi)^2}] \tag{A.12}$$

is the total Compton cross section on unpolarized electrons and $r_e = e^2/m_e c^2$. Remembering that the field of the optical beam is decreased quickly with the removal from the focus (it vanishes almost completely at $|z| > 4\pi cF^2/\omega a_0^2$), we calculate the integral in expression (A.11) the limits $-\infty < z < \infty$. Substituting expression (A.2) into expression (A.11) and using integral representation of the δ function:

$$\delta(y) = \frac{1}{2\pi} \int_{-\infty}^{\infty} \exp(iky) dk,$$

we obtain:

$$\int_{-\infty}^{\infty} |\tilde{E}(z,0)|^2 dz = 2\pi\omega \int_0^a \rho |\tilde{E}_0(\rho)|^2 d\rho = 4\pi\omega W/c^2, \tag{A.13}$$

where W is the total power of the optical beam. Thus, expression (A.11) for the probability of Compton scattering takes the form [4]:

$$P = 1 - \exp(-\delta), \qquad \delta = 2W\sigma_c/\hbar c^2. \tag{A.14}$$

Let us point at the important feature of this result. Under the condition (A.9), the expression for the probability of the Compton scattering (A.14) does not depend on the details of the optical field distribution on the focusing mirror and is defined by the total power of the laser beam. Applicability region of this result (see relation (A.10)) imposes the following restriction on the peak power of the laser radiation:

$$W \ll \frac{m_e^2 c^5}{e^2} \frac{F^2}{a_0^2} \frac{1}{(1+\chi)^2}.$$

When deriving expression (A.14) we have assumed the laser pulse duration to be infinitely long. Nevertheless, this expression is valid for the case of approximately equal lengths l_b and l_w of electron and laser beams. Taking into account expression (A.8) for axial dimension of the region with strong optical field, we may conclude that it takes place when

$$l_w \gg 4\pi c F^2/\omega a_0^2, \qquad l_b \lesssim l_w. \tag{A.15}$$

Spatial distribution of gamma quanta

All the above mentioned considerations are valid for an arbitrary value of parameter $\chi = 4\gamma\hbar\omega/m_e c^2$. From practical point of view two situations are of interest: $\chi \ll 1$ and $\chi \gg 1$. The first one describes classical limit of the Compton scattering and has been studied in detail elsewhere [6]. Here we consider the case of essentially quantum region of the Compton scattering, $\chi \gg 1$, which is the most suitable to describe the PLC of TeV energy range. So, in all the formulae we will assume that $\chi \gg 1$ and $\gamma \gg 1$.

To calculate the luminosity of the colliding $\gamma\gamma$ - beams, one should calculate spatial and energy distributions of the secondary γ - quanta $\rho_\gamma(\vec{r}, t)$. Differential cross-section of photon on unpolarized electron is of the form ($\gamma \gg 1$) [15]:

$$\frac{d\sigma_c}{\gamma^2 d\theta^2} = \frac{2\pi r_e^2}{(1+\chi+\gamma^2\theta^2)^2(1+\gamma^2\theta^2)} \left[\frac{\chi^2}{1+\chi+\gamma^2\theta^2} + \frac{2(1+\gamma^4\theta^4)}{1+\gamma^2\theta^2} \right].$$

When $\chi \gg 1$ and $\gamma^2\theta^2 \ll \chi$), this expression is reduced to:

$$\frac{d\sigma_c}{\gamma^2 d\theta^2} \simeq \frac{2\pi r_e^2}{\chi(1+\gamma^2\theta^2)}.$$

When parameter $\chi \gg 1$, the electron energy after the first scattering is of the order of $\mathcal{E}/\chi$, so we can neglect the process of multiple scattering and the spatial distribution of secondary gamma quanta may be written in the form:

$$dW \simeq \eta_{e\gamma} \frac{d\sigma_c}{\sigma_c d\theta^2} \frac{d\theta_x d\theta_y}{\pi},$$

where the conversion efficiency $\eta_{e\gamma}$ (i.e. the total number of γ - quanta produced by the single electron) is equal to:

$$\eta_{e\gamma} \simeq P = 1 - \exp(-\delta). \tag{A.16}$$

Interaction region

The main characteristic of the colliding beams is the luminosity L which is defined as

$$L = 2fN^{(1)}N^{(2)} \int \rho^{(1)}(\vec{r},t)\rho^{(2)}(\vec{r},t)d\vec{r}dt, \tag{A.17}$$

where $N^{(1,2)}\rho^{(1,2)}$ are the densities of the colliding beams ($\int \rho d\vec{r} = 1$) and f is the collision repetition rate. In the axisymmetric case, for the beams with the Gaussian distribution of the beam density we have:

$$\rho^{(1,2)}(r,z,t) = [(2\pi)^{3/2}\sigma_z\sigma_T^2(z)]^{-1} \exp[-\frac{r^2}{2\sigma_T^2(z)} - \frac{(z \mp Vt)^2}{2\sigma_z^2}], \tag{A.18}$$

where

$$\sigma_T(z) = \sigma_T(0)\sqrt{1+\frac{z^2}{\beta_0^2}}, \qquad \sigma_T(0) = \sqrt{\epsilon\beta_0/\pi},$$

ϵ is the electron beam emittance, σ_z is the width of the longitudinal distribution and β_0 is the beta-function at the interaction point. Substituting expression (A.18) into expression (A.17) we obtain:

$$L_{ee} = \frac{\sqrt{\pi}N_e^2 f}{8\epsilon\sigma_z} \exp(H^2)[1 - \frac{2}{\sqrt{\pi}} \int_0^H \exp(-x^2)dx], \tag{A.19}$$

where $H = \beta_0/\sigma_z$.

To obtain colliding gamma-quanta, one should convert high energy electrons into high energy gamma quanta (see previous section). When the distance z_0 between conversion point and interaction point is satisfied to the conditions:

$$\sigma_z \ll z_0, \qquad z_0 \ll \gamma\sigma_T^{(0)}/(1+\chi)^{1/2}, \tag{A.20}$$

and the conditions of the optimal focusing (A.9) and (A.15) are fulfilled, then γ - quantum beam density becomes proportional to the electron beam density:

$$N_\gamma \rho_\gamma = \eta_{e\gamma} N_e \rho_e(\vec{r}, t),$$

and the luminosity of the colliding $\gamma\gamma$ beams may be written in the form:

$$L_{\gamma\gamma} = \eta_{e\gamma}^2 L_{ee}. \tag{A.21}$$

Integral luminosity is not an exhaustive characteristic of the photon collider. From the practical point of view, the spectral luminosity, i.e. the luminosity calculated per unity frequency interval $\omega_0 = \sqrt{\omega_1\omega_2}$ of the colliding γ - quanta, is of a significant interest:

$$\frac{dL_{\gamma\gamma}}{d\omega_0} = 4 f N_\gamma^{(1)} N_\gamma^{(2)} \omega_0 \int_{\omega'}^{\omega''} \frac{d\omega_\gamma^{(1)}}{\omega_\gamma^{(1)}} \int d\vec{r} dt \frac{d\rho^{(1)}}{d\omega_\gamma^{(1)}} \frac{d\rho^{(2)}}{d\omega_\gamma^{(2)}}, \tag{A.22}$$

where $\omega_0 = \sqrt{\omega_\gamma^{(1)}\omega_\gamma^{(2)}}$, $\omega' = \omega_0^2/\omega_{max}$ and $\omega'' = \omega_{max} = \mathcal{E}\chi/(1+\chi)$. When the distance z_0 between the conversion and interaction point is rather small:

$$z_0 \ll \frac{\sigma_e^{(0)}}{\theta(\omega_\gamma)} = \frac{\gamma\sigma_e^{(0)}}{\sqrt{1+\chi}} \sqrt{\frac{\omega_0}{\omega_{max} - \omega_0}}, \tag{A.23}$$

then the spectral density of secondary gamma quanta becomes proportional to the electron density:

$$\frac{d\rho_\gamma}{d\omega_\gamma} \simeq \frac{\eta_{e\gamma}}{\sigma_c} \frac{d\sigma_c}{d\omega_\gamma} N_e \rho_e(\vec{r}, t), \tag{A.24}$$

where $\theta(\omega_\gamma)$ is given with expression (A.1). Substituting expression (A.24) into expression (A.22), one can obtain [4]:

$$\omega_0 \frac{dL_{\gamma\gamma}}{d\omega_0} = \eta_{e\gamma}^2 L_{ee} \frac{2\chi}{\ln^2\chi} \frac{\ln[1+2\chi(1-\nu)]}{1+\chi(1-\nu)}, \tag{A.25}$$

where $\nu = \omega_0/\omega_{max}$. It is seen from this expression that spectral luminosity has a sharp maximum in the vicinity of $(1-\nu) \sim 1/\chi$ which is achieved at $\nu \simeq 1 - 1.3/\chi$:

$$\omega_0 \left(\frac{dL_{\gamma\gamma}}{d\omega_0}\right)_{max} \simeq 1.1\, L_{ee} \frac{\eta_{e\gamma}^2 \chi}{\ln^2 \chi}. \tag{A.26}$$

An application of the FEL as a laser for PLC reveals wide possibilities to steer the polarization of the colliding photon beams. In the FEL amplifier, the polarization of the amplified wave is defined by the undulator magnetic field configuration. For instance, in the case of the helical undulator, the output FEL radiation is circularly polarized. As a result, one can easily steer the polarization of the colliding $\gamma\gamma$ - beams.

Let us consider the practically important case when the FEL optical beam is circularly polarized and electron beam is unpolarized. In essentially quantum region, $\chi \gg 1$, the differential Compton cross section averaged over final polarization states of electron is given with the expression [4]:

$$\frac{d\sigma_c}{d\omega_\gamma} = \frac{\pi r_e^2 \hbar}{\chi(\mathcal{E} - \hbar\omega_\gamma)} \left[1 + \xi_{opt}\xi_\gamma \left(1 - \frac{2\hbar\omega_\gamma}{\chi(\mathcal{E} - \hbar\omega_\gamma)}\right)\right].$$

At the given helicity of the optical beam ξ_{opt}, the helicities of the backscattered γ - quanta may take the values ± 1. As a result, the total luminosity may be presented as a sum of partial luminosities corresponding to the different helicity combinations of colliding γ - quanta. In the essentially quantum region, $\chi \gg 1$, and at small distance between the conversion and interaction point (see relation (A.23)), we obtain the following expression for spectral luminosity [4]:

$$\omega_0 \frac{dL_{\gamma\gamma}}{d\omega_0} = \eta_{e\gamma}^2 L_{ee} \frac{2\chi}{\ln^2 \chi} f(\nu, \xi^{(1)}, \xi^{(2)}), \tag{A.27}$$

where $\xi^{(1,2)} = \xi_{opt}^{(1,2)} \xi_\gamma^{(1,2)}$ are the products of the helicities of incident and scattered photons. Function $f(\nu, \xi^{(1)}, \xi^{(2)})$ is given with the following expressions:

$$\begin{aligned}
f(\nu,1,1) &= \frac{1}{(1+k)^2}\left[\left(2k + \frac{1}{1+k}\right)\ln(1+2k) - 2k\right], \\
f(\nu,1,-1) &= f(\nu,-1,1) = \frac{1}{(1+k)^2}\left[\frac{k}{1+k}\ln(1+2k) + \frac{2k^2}{1+2k}\right], \\
f(\nu,-1,-1) &= \frac{1}{(1+k)^2}\left[\frac{\ln(1+2k)}{1+k} + \frac{2k}{1+2k}\right],
\end{aligned} \tag{A.28}$$

where $k = \chi(1-\nu)$. It is seen from these expressions that the photon collider may be easily tuned on the required partial luminosity maximum by steering of the FEL optical beam polarization.

Final remark

In conclusion of this section it should be noted that all the presented above formulae refer to the case of the laser beam with ideal (i.e. diffraction limited) dispersion. In other words, the phase volume of the laser beam was assumed to be of the order of radiation wavelength λ. In the case when the laser beam phase volume exceeds significantly this value, the required laser power should be increased significantly to achieve a desired value of the conversion efficiency. In connection with this we should emphasize that the phase volume of radiation of powerful lasers usually exceeds by several tens of magnitude the value of λ. The main effect which determines the growth of the radiation dispersion is fluctuations of the active medium refractive index due to thermal effects. Contrary to this, the radiation of the FEL amplifier has always minimal phase volume because the process of the field amplification develops in vacuum.

B Diaphragm focusing line

As a rule, lens systems are used for transporting and focusing of optical radiation. While this technique is appropriate at a relatively small radiation power, it is completely unfit for focusing and transporting of powerful laser beams with high the average and peak radiation power. Nevertheless, this problem may be solved by using diaphragm focusing line which has a form of periodically spaced screens with round holes.

Diaphragm focusing line operates as follows. Consider electromagnetic wave passing along the sequence of diaphragm. When electromagnetic wave diffracts at the first diaphragm, it produces diffraction pattern in the plane of the next diaphragm. When the second diaphragm is placed in the main maximum of the diffraction pattern, diffraction losses are minimal. Further, sideband maxima of the diffraction pattern produced by the second diaphragm are less than that of the first pattern, etc. When the wave passes a large number of diaphragms, the field eigenmode is formed which has low diffraction losses. For the first time eigenmodes of the diaphragm line have been calculated numerically by Fox and Li [18] and later have been obtained analytically by Veinstein [16].

To get a deeper insight into the role of diffraction effects for forming the eigenmode in the diaphragm line, we, following by ref. [19], study the problem of

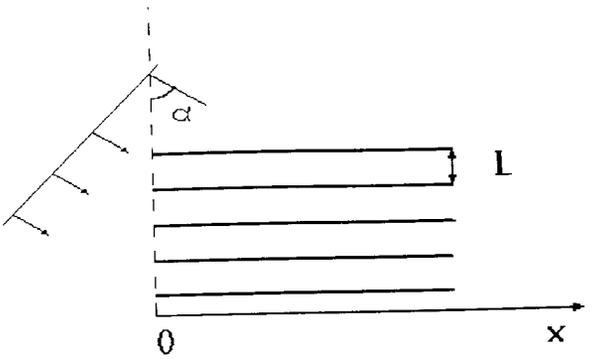

Fig. B.1. Diffraction of plane wave at semi-infinite screens (see explanations in the text).

the diffraction of the plane wave at periodical sequence of completely absorbing semi-infinite screens (see Fig.C.1). Period of the structure is equal to L and direction of the wave propagation forms a small angle α with the plane perpendicular to the edges of the screens. We assume that

$$\alpha^2 \ll \lambda/(\pi L),$$

where λ is the wavelength.

The field of the wave, diffracted at the edge of totally absorbing screen, can be presented as a sum of two waves: the wave which does not exist in the region of geometrical shadow and is unperturbed outside it, and cylindrical wave which is produced by a image source located at the edge of the screen [20]. In the considered geometry, the field $u_1(x)$ of the wave, diffracted at the first screen is given with the expressions:

$$u_1(x) = \begin{cases} u_0 - (u_0/\pi^{1/2})F(\xi), & x < 0 \\ (u_0/\pi^{1/2})F(\xi), & x > 0 \end{cases} \tag{B.1}$$

where u_0 is the amplitude of incident plane wave,

$$F(\xi) = \int_{\xi}^{\infty} \exp(i\tau^2)d\tau$$

is Fresnel integral and $\xi = (\pi/\lambda L)^{1/2}x$. Substituting approximate expression for Fresnel integral

$$F(\xi) = i\exp(i\xi^2)\left[2\left[\xi + \sqrt{i/\pi}\right]\right]^{-1}$$

into formula (B.1) for $u_1(x)$ we obtain the field distribution in the region of geometrical shadow:

$$u_1(x) \simeq A(x) \exp(ikx^2/2L),$$

where $k = 2\pi/\lambda$ and $A(x)$ is slowly changing function.

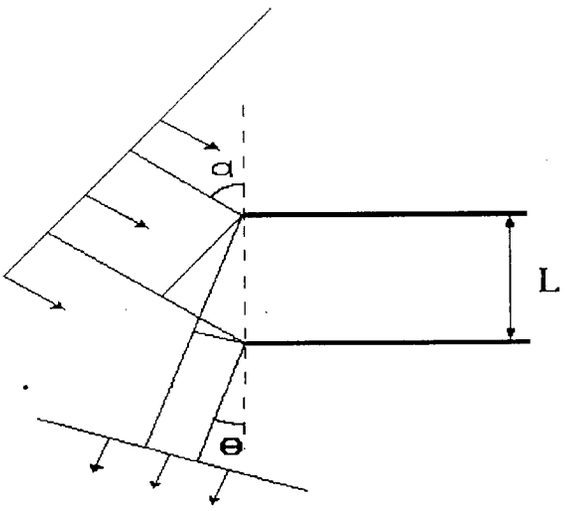

Fig. B.2. Diffraction of plane wave at semi-infinite screens (see explanations in the text).

When unperturbed wave is diffracted at the second edge, it produces another cylindrical wave with the image source located at the edge of the second screen. Besides this wave, there exists also unperturbed plane wave which produces another cylindrical wave at the third screen, etc. As a result, the field of diffracted wave is presented in the region $x < 0$ by a superposition of cylindrical waves produced by image sources located at the edges of all the screens and with amplitudes decreasing with the deflection of their propagation off the direction of propagation of the initial wave (see Fig.C.2).

Due to the interference of a large number of cylindrical waves, there exists a series of discrete directions where amplitudes of these waves are summed. The waves produced by edges of the adjacent screens are summed when

$$kL(\theta^2 - \alpha^2)/2 \simeq 2\pi n,$$

where n is integer number. At the intermediate directions, the field amplitude takes zero value due to interference effects. At $\alpha^2 \ll \lambda/(\pi L)$ the amplitude of the "reflected" wave with $n = 0$ and $\theta_0 = \alpha$ significantly exceeds the amplitudes of another waves.

So, when the incident angle of the wave is rather small, ($\alpha^2 \ll \lambda/(\pi L)$), the radiation does not absorb and is dispersed due to diffraction effects and the most fraction of the power is in the "reflected" wave.

Using analytical techniques, Veinstein has obtained coefficient of diffraction reflection R_0 of the plane wave from the sequence of semi-infinite periodical screens [16]:

$$R_0 = -\exp\left[-\beta_0(1-i)s\right], \tag{B.2}$$

where $s = \alpha(kL)^{1/2}$ and $\beta_0 = 0.824$. When factor s is decreased, the absolute value of R_0 is approached to the unity. The phase multiplier in the right-hand part of eq. (B.2) corresponds to the phase shift not equal to π. As a result, the process of reflection takes place as if a mirror should be placed slightly farther then the plane of the screen edges.

Let us derive one important consequence of eq. (B.2). Resulting field of incident and reflected wave may be presented in the form:

$$E(x,z,t) = u(x)\exp(ikz - i\omega t) = \\ [A\exp(ik_x x) + B\exp(-ik_x x)]\exp(ikz - i\omega t),$$

where $k_x/k_z \simeq \alpha$, $k_x^2 + k_z^2 = 4\pi^2/\lambda^2$ and $\omega = 2\pi c/\lambda$. At the plane of the screen edges the ratio of reflected and incident waves B/A is equal to R_0, which results in

$$u(x) = A\left[\exp(ik_x x) \quad + \quad R_0\exp(-ik_x x)\right].$$

One can obtain that the value of logarithmic derivation of $u(x)$ at the plane of the screen edges is equal to:

$$d\ln(u)/dx|_{x=0} = (1/u)du/dx|_{x=0} = ik_x(1-R_0)/(1+R_0).$$

Assuming factor s to be small and replacing $\exp\left[-\beta_0(1-i)s\right]$ by $1-\beta_0(1-i)s$, we obtain

$$(1-R_0)/(1+R_0) \simeq \left[\beta_0(1-i)k_x\sqrt{\lambda L/(8\pi)}\right]^{-1},$$

and

$$d\ln(u)/dx|_{x=0} = -\left[\beta_0(1+i)\sqrt{\lambda L/(8\pi)}\right]^{-1}. \tag{B.3}$$

Peculiar feature of the latter formula is that the term k_x is completely excluded from it, which allow one to use it as a universal boundary condition. Let us consider, for instance, a periodical diaphragm line formed by a sequence of slits in absorbing screens. Transverse dimension of the slits is equal to $2a$ and coordinates of the screen edges are equal to $x = \pm a$. Eigenfunctions $u_j(x)$ of such a diaphragm line are the solutions of the homogeneous equation:

$$d^2u_j/dx^2 + k_j^2 u_j = 0$$

and satisfy boundary conditions

$$\left[u_j \pm (1+i)\beta_0\sqrt{\lambda L/(8\pi)}du_j/dx\right]_{x=\pm a} = 0.$$

In the first approximation of a small parameter $M = (8\pi N_F)^{-1/2}$, where $N_F = a^2/(\lambda L)$ is Fresnel number, functions u_j are given with

$$u_j(x) = \begin{cases} \cos[\pi j(1-\Delta)x/(2a)], & j = 1,3,\ldots \\ \sin[\pi j(1-\Delta)x/(2a)], & j = 2,4,\ldots \end{cases} \tag{B.4}$$

where $\Delta = (1+i)\beta_0 M$. Validity region of these results is that parameter j must satisfy inequality

$$\pi^2 j^2 M^2 \ll 1.$$

Substituting $k_x = \pi j(1-\Delta)/(2a)$ into relation

$$k_x^2 + k_z^2 = \omega^2/c^2 = 4\pi^2/\lambda^2$$

we obtain expression for k_z:

$$k_z L \simeq \omega L/c - \pi^2 j^2 M^2/2 + \pi^2 j^2 M^3(1+i)\beta_0.$$

For the j-th eigenmode, a fraction of the radiation power losses per passage of one diaphragm is given with the relation:

$$2\,\mathrm{Im}(k_z L) = 2\pi^2 j^2 \beta_0 M^3.$$

Axisymmetric diaphragm line

On the base of previous study we can calculate parameters of the axisymmetric diaphragm line. We assume the radius of the hole to be rather large, $R \gg \lambda$. Eigenfunctions $\Phi_m(r,\varphi)$ of the axisymmetric diaphragm line have the form:

$$\Phi_m = \Phi_{mj}(r)\exp(-\mathrm{im}\varphi), \qquad m = 0, 1, 2, \ldots$$

Functions Φ_{mj} are the solutions of the homogeneous equation:

$$r^2 d^2\Phi_{mj}/dr^2 + r d\Phi_{mj}/dr + (k_{mj}^2 - m^2)\Phi_{mj} = 0 \tag{B.5}$$

and satisfy boundary conditions:

$$\left[\Phi_{mj} + (1+i)\beta_0\sqrt{\lambda L/(8\pi)}\, d\Phi_{mj}/dr\right]_{r=R} = 0. \tag{B.6}$$

In the first order of a small parameter $M = (8\pi N_F)^{-1/2}$, where $N_F = R^2/(\lambda L)$ is Fresnel number, functions Φ_{mj} have the form [16], [19], [21]:

$$\Phi_{mj} = J_m(k_{mj}r),$$

where $k_{mj} = \nu_{mj}(1-\Delta_0)/R$, $\Delta_0 = (1+i)\beta_0 M$, ν_{mj} is j-th root of the Bessel function of the m-th order (i.e. $J_m(\mu_{mj}) = 0$). Substituting expressions for k_{mj} into relation

$$k_z^2 + k_{mj}^2 = \omega^2/c^2$$

we obtain expression for k_z :

$$k_z L \simeq \omega L/c - 2\mu_{mj}^2 M^2 + 4\nu_{mj}^2 M^3(1+i)\beta_0.$$

For the TEM_{mj} eigenmode, a fraction of the radiation power losses per passage of one diaphragm is given with the relation:

$$2\,\mathrm{Im}(k_z L) = \delta\mu_{mj}^2 M^3\beta_0. \tag{B.7}$$

Imperfections of diaphragm line

Let us study the influence of imperfections in the diaphragm line on its properties (see. e.g. ref. [19]).

When one of the screens is shifted off the axis, it may cause distortion of the amplitude and phase of the scattered wave. To estimate the change in the amplitude, one should remember that the amplitude of the cylindrical wave, produced by the edge of the screen, is proportional to the Fresnel integral $F(\xi)$ in the region of the next screen and is decreased by a factor of 2.5 at $\mid x \mid > (\lambda L/\pi)^{1/2} = \Delta_1$. So, the region of $x > \Delta_1$ is the region of shadow. If the screen is shifted off the axis by the value $\delta \gtrsim \Delta_1$, either this screen or the next screen falls into the region of the shadow and does not produce diffracted wave.

To estimate phase errors, we consider the drawing presented in Fig.C.2. One can see that the shift of the screen by the value δx in the transverse direction causes the phase shift of the wave, propagated by the angle θ

$$k\delta x(\sin\alpha + \sin\theta) \simeq k\delta x(\alpha + \theta).$$

For the reflected wave, the change in the phase equal to π is achieved at $\delta x = \Delta_2 = \lambda/(4\alpha)$. At small angle approximation $\alpha^2 \ll \lambda/(\pi L)$, it results in the inequality $\Delta_2 \gg \Delta_1$ which means that the value of admissible shift of the screen is defined mainly by aperture restrictions but not by phase distortions. So, requirements on the accuracy of transverse adjustment of the screens is given with $\delta x \ll \Delta_1 = (\lambda L/\pi)^{1/2}$.

As for the accuracy of the longitudinal adjustment of the screens, it is defined mainly by the effect of the higher order modes production. A relative power of this effect is given with the ratio of the error in the period δL to the period L. When the screens are adjusted with the accuracy about of $\delta L \simeq 10^{-2}$ cm, an irregularity of the diaphragm focusing line does not result in the extra diffraction losses.

In conclusion of this section it should be noticed that there is no need to use completely absorbing screens in the diaphragm line. Moreover, it would be preferable to use reflecting screens. At accepted limitations, reflecting screens are almost identical to absorbing screens with respect to diffraction effects, while the problems of the heat load on the edges of diaphragms are not so severe.

C Rigorous results of the linear theory of FEL amplifier with focusing diaphragm line

When FEL driving beam has relatively low value of the peak beam current, there is no possibility to use conventional FEL amplifier scheme in which radiation is confined due to "optical guiding" effect [9,10]. To overcome this

problem, an FEL amplifier with diaphragm focusing line could be used [11]. Diaphragm focusing line has a form of periodically spaced screens with round holes and confines the radiation in the vicinity of the electron beam (see Appendix C).

The analyzed model of the FEL amplifier is based on the Maxwell wave equation taken in a paraxial approximate form and on the description of particle motion by a kinetic equation expressed in "energy-phase" variables. It is anticipated that electrons move (averaged over constrained motion) only along trajectories parallel to the undulator axis.

In the linear high-gain limit the radiation of the electron beam in the undulator can be represented as a set of modes. When amplification takes place, the mode configuration in the transverse plane remains unchanged while the amplitude grows with the undulator length exponentially. Each mode is characterized with the increment eigenvalue and the field distribution eigenfunction in terms of transverse coordinates. The mode with the highest increment has the advantage over all other modes. Following the gain process along the undulator axis one can find that the field distribution is settled corresponding to the mode with the maximal increment.

To find eigenvalues and eigenfunctions of the beam radiation modes we use the following boundary conditions:
a) the continuity requirement of the eigenfunction and its derivative must be fulfilled at the electron beam boundary.
b) To take into account diffraction effects in the diaphragm line, the rigorous impedance boundary conditions are applied at the edges of the diaphragms (proposed by L.A Veinstein [16]).

As a result, it possible to reduce the problem of the open waveguide to the closed one and we then get the equations which may be resolved analytically by standard methods.

Such a model enables one to take into account diffraction effects and energy spread of the particles in the beam. Despite its relative simplicity, it describes rather well the FEL systems in which the transverse size of the electron beam is much less than the transverse dimensions of the field eigenmode (it is just the same situation which takes place for the FEL amplifier considered in section 3).

Basic equations

First, we consider electrodynamic problem. The electromagnetic field in the FEL amplifier is subjected to the wave equation:

$$c^2\nabla^2\vec{E} - \partial^2\vec{E}/\partial t^2 = c^2\vec{\nabla}(\vec{\nabla} \circ \vec{E}) + 4\pi\partial\vec{j}/\partial t, \tag{C.1}$$

which can be obtained from Maxwell's equations. In the paraxial approximation, we can ignore the summand contribution $c^2\vec{\nabla}(\vec{\nabla} \circ \vec{E})$ on the right-hand side of eq. (C.1). We consider the case when transverse motion of the electrons is defined totally by the undulator field and the longitudinal velocity of electrons is close to the velocity of light c, so the transverse component of the beam current density can be written in the form:

$$\vec{j}_\perp = \theta_w\,[\,\vec{e}_x\cos(\kappa_w z) - \vec{e}_y\sin(\kappa_w z)\,]\,(\,\tilde{j}_1 e^{i\psi} + C.C.\,), \tag{C.2}$$

where $\tilde{j}_1$ is the complex amplitude of the first harmonic of the beam current. We seek the solution for $\vec{E}$ in the form of eq. (2) where we explicitly segregated the strong dependence of E on the z coordinate. Substituting eqs. (2) and (C.2) into eq. (C.1) and neglecting fast oscillating terms, we obtain the equation for slowly changing amplitudes $\tilde{j}_1$ and $\tilde{E}$:

$$c^2\,[\,\nabla_\perp^2 + 2i(\omega/c)\partial/\partial z\,]\,\tilde{E} = -4\pi i\theta_w\omega\tilde{j}_1, \tag{C.3}$$

where $\nabla_\perp^2$ is Laplace operator in transverse coordinates. In the paraxial approximation, the characteristic scale of the field amplitude $\tilde{E}$ change is much more than the radiation wavelength, so in eq. (C.3) we have omitted the second order derivative of $\tilde{E}$ over z.

To obtain self-consistent approach, we should find the motion of the electrons in the given electromagnetic field. We describe the motion of electrons using the "energy - phase" variables $\mathcal{E}$ and $\psi = \kappa_w z + \omega(z/v_{ph} - t)$. Using the approximation that electrons move only in the z direction, and writing down the distribution function $f(\psi, \mathcal{E}, z, \vec{r}_\perp)$ in the linear approximation:

$$f = f_0 + \tilde{f}_1 e^{i\psi} + \tilde{f}_1^* e^{-i\psi}, \tag{C.4}$$

we write the following equation for $\tilde{f}_1$ [10]:

$$\partial\tilde{f}_1/\partial z + i\,[\,C + \omega P/(c\gamma_z^2)\,]\,\tilde{f}_1 - (e\theta_w\tilde{E}/2\mathcal{E}_0)\partial f_0/\partial P = 0. \tag{C.5}$$

Complex amplitude $\tilde{j}_1$ is connected with $\tilde{f}_1$ as

$$\tilde{j}_1 \simeq -ec \int \tilde{f}_1 dP,$$

Using initial conditions

$$\tilde{f}_1|_{z=0} = 0, \qquad f_0|_{z=0} = n_0(\vec{r}_\perp)F(P), \tag{C.6}$$

where the function $F(P)$ describing the energy distribution is normalized to the unity, we can obtain solution for $\tilde{j}_1$ by integration of eq. (C.5). Substituting the obtained result into right-hand side of eq. (C.3), we obtain the only integro-differential equation for the field amplitude $\tilde{E}$:

$$c^2 \left[\nabla_\perp^2 + \frac{2i\omega}{c}\frac{\partial}{\partial z}\right] \tilde{E}(z,\vec{r}_\perp) = 2\pi i e\theta_w^2 \omega j_0(\vec{r}_\perp) \int_0^z dz' \tilde{E}(z',\vec{r}_\perp) \times$$
$$\int dP \frac{dF}{dP} \exp\left[i\{C + \frac{\omega P}{c\gamma_z^2}\}(z'-z)\right], \tag{C.7}$$

where $-j_0(\vec{r}_\perp) \simeq -ecn_0(\vec{r}_\perp)$ is the longitudinal component of the beam current density at the undulator entrance at $z = 0$.

Boundary conditions

First, the continuity requirement of the field and its derivative must be fulfilled at the beam boundary. Second, diffraction effects at the edges of diaphragm line should be taken into account. The first investigation of the diffraction effects influence on the forming of the field eigenmodes in the diaphragm line was carried out by Fox and Li using Huygens' principle [18]. Here we use more rigorous approach. In the diaphragm line the diffraction effects on the edges can be taken into account using method by L.A. Veinstein [16]. He had shown that when the radiation wavelength is much less than all characteristic dimensions of the diaphragm line, the following boundary condition can be imposed at the edges of the diaphragm line:

$$\tilde{E} + 0.824(1+i)\,[\,cL/4\omega\,]^{1/2}\,\partial\tilde{E}/\partial\zeta = 0, \tag{C.8}$$

where ζ is the direction of the normal to the imaginary side surface of the waveguide. At the accepted limitations this boundary condition is independent of the polarization of the radiation.

Therefore, the problem concerning the open waveguide excitation by means of equivalent boundary conditions is reduced to a more usual classical formulation of the problem of the closed waveguide excitation.

Solution of the eigenvalue problem

Let us consider the FEL amplifier with an axisymmetric homogeneous electron beam of radius r_0. In the high gain limit we solve eq. (C.7) by the separation of variable method. Using polar coordinates (r, φ, z) we seek the solution for $\tilde{E}$ in the form:

$$\tilde{E}(r,\varphi,z) = \Phi_{\rm n}(r)\exp(\Lambda z)\begin{pmatrix}\cos(n\varphi)\\ \sin(n\varphi)\end{pmatrix}, \tag{C.9}$$

where n is integer, $n \geq 0$. Substituting expressions (C.9) into eq. (C.7), we obtain the Bessel equations:

$$\hat{r}^2 d^2\Phi_{\rm n}/d\hat{r}^2 + \hat{r}d\Phi_{\rm n}/d\hat{r} + \left[\mu^2\hat{r}^2 - n^2\right]\Phi_{\rm n} = 0, \qquad \text{at} \qquad \hat{r} < 1, \tag{C.10a}$$

$$\hat{r}^2 d^2\Phi_{\rm n}/d\hat{r}^2 + \hat{r}d\Phi_{\rm n}/d\hat{r} - \left[g^2\hat{r}^2 + n^2\right]\Phi_{\rm n} = 0, \qquad \text{at} \qquad \hat{r} > 1, \tag{C.10b}$$

where $\hat{r} = r/r_0$. $\hat{C} = C/\Gamma$, $g^2 = -2iB\hat{\Lambda}$, $\hat{\Lambda} = \Lambda/\Gamma$,

$$\mu^2 = -2i\hat{D}\Lambda - g^2, \qquad \hat{D} = \int_{-\infty}^{\infty} \frac{d\hat{F}(\xi)/d\xi}{(\hat{\Lambda} + i\hat{C}) + i\xi} d\xi. \tag{C.11}$$

The distribution function $\hat{F}(\hat{P})$ with

$$\hat{P} = (\mathcal{E} - \mathcal{E}_0)/\beta\mathcal{E}_0, \tag{C.12}$$

is normalized to the unity, $\int \hat{F}(\xi)d\xi = 1$, $\beta = c\gamma_z^2\Gamma/\omega$. The gain parameter Γ and diffraction parameter B are given with the expressions:

$$\Gamma = \left[\frac{I\omega^2\theta_{\rm w}^2}{I_A c^2 \gamma_z^2 \gamma}\right]^{1/2}, \qquad B = \Gamma r_0^2\omega/c. \tag{C.13}$$

When the energy spread is Gaussian, the function $\hat{D}$ is given with the expression:

$$\hat{D} = i \int_0^\infty \xi \exp\left[-\hat{\Lambda}_T^2 \xi^2/2 - (\hat{\Lambda} + i\hat{C})\xi\right] d\xi, \tag{C.14}$$

where $\hat{\Lambda}_T^2 = \sigma^2/\beta^2\mathcal{E}_0^2$ is the energy spread parameter.

Let us consider the region inside the beam. To avoid the singularity of the solution at $r = 0$, the solution of eq. (C.10a) should be chosen in the form:

$$\Phi_n = C_1 J_n(\mu r/r_0) \qquad \text{at} \quad r < r_0. \tag{C.15a}$$

Solution of eq. (C.10b) for Φ_n must be chosen in the form:

$$\Phi_n = C_2 I_n(gr/r_0) + C_3 K_n(gr/r_0) \qquad \text{at} \quad r_0 < r < R. \tag{C.15b}$$

Fulfillment of the boundary condition at the edge of the diaphragm line

$$\left[\Phi_n(r) + 0.824(1+i)\sqrt{cL/4\omega}\, d\Phi_n/dr\right]_{r=R} = 0, \tag{C.16}$$

and continuity requirements of Φ_n and $d\Phi_n/dr$ at the beam boundary lead to the system of three linear equations for three coefficients C_1, C_2 and C_3. To obtain nontrivial solution, its determinant should be set equal to zero which results in the eigenvalue equation for the FEL amplifier with diaphragm line:

$$gK_{n+1}(g)J_n(\mu) - \mu J_{n+1}(\mu)K_n(g) + [gI_{n+1}(g)J_n(\mu) + \mu J_{n+1}(\mu)I_n(g)]\frac{K_n(\chi)}{I_n(\chi)} = 0. \tag{C.17}$$

The field eigenmode (field distribution over radius) has the form:

Region 1 ($\hat{r} < 1$):

$$\Phi_n(\hat{r}) = J_n(\mu\hat{r}) \tag{C.18a}$$

Region 2 ($1 < \hat{r} < \sqrt{\Omega/B}$):

$$\Phi_n(\hat{r}) = \frac{J_n(\mu)\,[K_n(g\hat{r}) - I_n(g\hat{r})K_n(\chi)/I_n(\chi)]}{K_n(g) - I_n(g)K_n(\chi)/I_n(\chi)}, \tag{C.18b}$$

where the following notations have been introduced:

$$\chi = g(1+\Delta)\sqrt{\Omega/B}, \quad \Delta = 0.824(1+i)M, \quad M = \sqrt{cL/4\omega R^2}, \qquad (C.19)$$

$\Omega = \Gamma R^2\omega/c$ is the waveguide diffraction parameter. In the further consideration we assume the Fresnel number of diaphragm line to be a large value, i.e we assume that $M \ll 1$.

It should be noted that each mode is double degenerated at $n > 0$, because for each value of azimuthal number $n > 0$ there are two linearly independent functions:

$$\Phi = \Phi_{\rm n}(\hat{r})\cos(n\varphi) \qquad \text{and} \qquad \Phi = \Phi_{\rm n}(\hat{r})\sin(n\varphi). \qquad (C.20)$$

Let us present the expansion of the field eigenmode in a series of empty waveguide eigenmodes. Eigenmodes of axisymmetric diaphragm line are the solutions of homogeneous equation (B.5) and satisfy boundary condition (B.6). Eigenfunctions Φ_{nj} are orthogonal in the sense that

$$\int_0^{\sqrt{\Omega/B}} \Phi_{nk}(\hat{r})\Phi_{nj}(\hat{r})\hat{r}d\hat{r} = 0 \qquad \text{at} \qquad k \neq j. \qquad (C.21)$$

It should be noted that the condition of orthogonality is formulated without complex conjugation. Eigenfunctions of empty waveguide $\Phi_{nj}(\hat{r})$ form a full basis, so the eigenfunction of active waveguide $\Phi_{\rm n}(\hat{r})$ can be expanded in a series

$$\Phi_{\rm n}(\hat{r}) = \sum_j A_{nj}\Phi_{nj}(\hat{r}). \qquad (C.22)$$

Using orthogonality condition for Φ_{nj} and omitting inessential common factor, we find the coefficients of expansion:

$$A_{nj} = \left[k_{nj}^2 r_0^2 + g^2\right]^{-1} \int_0^1 \Phi_{\rm n}(\hat{r})\Phi_{nj}(\hat{r})\hat{r}d\hat{r}. \qquad (C.23)$$

In the first order of small parameter M, functions Φ_{nj} have the form:

$$\Phi_{nj} = J_n(k_{nj}r)/J_{n+1}(\mu_{nj}), \qquad (C.24)$$

where $k_{nj} = \nu_{r,j}(1-\Delta)/R$, ν_{nj} is the jth root of the Bessel function of order n. Using expressions (C.23) and (C.24), we find with the accuracy of an order

of M the coefficients of expansion A_{nj} $(n = 0, 1, 2 \ldots)$:

$$A_{nj} = \frac{\mu J_{n+1}(\mu) J_n(\hat{k}_{nj}) - \hat{k}_{nj} J_n(\mu) J_{n+1}(\hat{k}_{nj})}{\left[g^2 + \hat{k}_{nj}^2\right] \left[\mu^2 - \hat{k}_{nj}^2\right] J_{n+1}(\nu_{nj})}, \tag{C.25}$$

where $\hat{k}_{nj} = k_{nj} r_0 = \nu_{nj}(1 - \Delta)\sqrt{B/\Omega}$. The relative contribution of the power of passive waveguide modes into the power of active waveguide mode can be written as

$$W_j / W = \mid A_{nj} \mid^2 \left[\sum_k \mid A_{nk} \mid^2\right]^{-1}. \tag{C.26}$$

Let us define the increment of radiation mode as the real part of the eigenvalue. When the undulator is long enough, the radiation mode with the highest increment has an advantage over all other modes. At small values of the waveguide diffraction parameter Ω, when $\Omega \sim 1$, these dependencies have a character of maxima series (see Fig.9). The physical nature of this phenomenon is illustrated with the plot presented in Fig.10 where a histogram of the relative contributions of the passive waveguide modes into the power of the beam radiation mode, is presented. One can find from this plot that each time when the resonant condition of the beam with the corresponding passive waveguide mode is fulfilled, the contribution of the latter to the beam radiation mode becomes dominating at small values of waveguide diffraction parameter Ω. We will show below that this case is rather well described by a single-mode approximation. At the higher values of the diffraction parameter Ω the width of the resonances becomes comparable with the distance between them and several waveguide modes begin at once to contribute to the radiation beam mode. Finally, when aperture of the diaphragm line becomes to be rather large, i.e. at $\Omega \gg 1$, the dependence of the increment on the detuning becomes smooth and the open beam approximation becomes valid [10].

Let us now study in details the asymptote of dispersion equation (C.17) corresponding to the single-mode approximation and the open beam asymptote.

Open beam asymptote

This asymptote corresponds to the case when the diaphragm aperture is rather large, i.e. we should let $\Omega \to \infty$ in equation (C.17). Using asymptotic expansion of the Bessel functions at large values of argument (it is assumed that $\mathrm{Re}(g) > 0$):

$$I_n(\zeta) \to (2\pi\zeta)^{-1/2} \exp(\zeta), \qquad K_n(\zeta) \to (2\zeta/\pi)^{-1/2} \exp(-\zeta) \tag{C.27}$$

we find that

$$K_n(\chi)/I_n(\chi) \to 0 \qquad \text{at} \qquad \Omega \to \infty. \tag{C.28}$$

and finally obtain dispersion equation for the open axisymmetric beam [10]:

$$gK_{n+1}(g)J_n(\mu) - \mu J_{n+1}(\mu)K_n(g) = 0. \tag{C.29}$$

Single-mode approximation

This asymptote corresponds to the case when the gain parameter Γ is rather small, $\Gamma \to 0$. It could take place, for example, when the beam current I is rather small, i.e. at $I \to 0$. So, we should let $B \to 0$, $\Omega/B = \text{const}$ and $\Lambda/\Gamma \to \infty$. In zeroth approximation we obtain $\mu = ig$ and equation (C.17) transforms to:

$$J_n\left(\mu(1+\Lambda)\sqrt{\Omega/B}\right) = 0. \tag{C.30}$$

For zeroth approximation of the eigenvalue we get:

$$\hat{\Lambda} = -i\nu_{nk}^2(1-2\Delta)/2\Omega. \tag{C.31}$$

Expressing $\hat{\Lambda}$ as $\hat{\Lambda} = -i\nu_{nk}^2(1-2\Delta)/2\Omega + \hat{\Lambda}_1$, where $\hat{\Lambda}_1$ is small, in the first order of $\hat{\Lambda}_1$ and in the case of negligibly small energy spread we obtain the eigenvalue equation of the single-mode approximation for TEM_{nk} mode:

$$(\hat{\Lambda} + i\hat{C})^2\,[\,\hat{\Lambda} + i\nu_{nk}^2(1-2\Delta)/2\Omega\,] = i\,[\,(1-2\Delta)/\Omega J_{n+1}(\nu_{nk})\,]\,[\,J_n^2(\hat{k}_{nk}) - J_{n-1}(\hat{k}_{nk})J_{n+1}(\hat{k}_{nk})\,] \tag{C.32}$$

Fig.9 illustrates an accuracy of the single-mode approximation at a small value of the waveguide diffraction parameter Ω.

References

[1] Status reports on TESLA, DLC, NLC, JLC and VLEPP are given in: Proceedings of the LC'92 ECFA Workshop on e^+e^- Linear Colliders (July, 25 – August , 2, 1993, Germany), MPI-PhE/93-14, ECFA 93-154

[2] D.L. Borden, D.A. Bauer and O. Caldwell, SLAC-PUB-5715 (January, 1992)

[3] I.F. Ginzburg et al., Pis'ma v ZhETF **34**(1981)514, Preprint INF 81-50, Novosibirsk (1981), in Russian

[4] A.M. Kondratenko, E.V. Pakhtusova and E.L. Saldin, Dokl. Akad. Nauk **264**(1982)849. Preprint INF 81-130, Novosibirsk (1981), in Russian

[5] V.I. Telnov, Nucl. Instrum. and Methods **A294**(1990)72

[6] E.L. Saldin, V.P. Sarantsev, E.A. Schneidmiller and M.V. Yurkov, Nucl. Instrum. and Methods **A339**(1994)583

[7] E.L. Saldin, V.P. Sarantsev, E.A. Schneidmiller and M.V. Yurkov, "Photon Linear Colliders of TeV Energy Range", Preprint JINR E-9-94-74, Dubna, 1994. Submitted to Particle Accelerators

[8] M. Tigner, Proceedings of the LC'92 ECFA Workshop on e^+e^- Linear Colliders (July, 25 – August , 2, 1993, Germany), MPI-PhE/93-14, ECFA 93-154, p.227

[9] G.T. Moore, Optics Communications **52**(1984)46

[10] E.L. Saldin, E.A. Schneidmiller and M.V. Yurkov, Optics Communications, **97**(1993)272

[11] E.L. Saldin, V.P. Sarantsev, E.A. Schneidmiller, Yu.N. Ulyanov and M.V. Yurkov, "Free electron laser as energy driver for inertial confinement fusion ", Preprint JINR E-9-94-237, Dubna, 1994. Submitted to Nuclear Instruments and Methods A

[12] N. Ohigashi et al., Nucl. Instrum. and Methods **A341**(1994)426

[13] Proceedings of the Third Workshop on Japan Linear Collider (JLC) (KEK, February 18-20, 1992), KEK Proceedings 92-13, 1992.

[14] E.L. Saldin, E.A. Schneidmiller and M.V. Yurkov, Sov. J. Part. Nucl. **23**(1992)104

[15] V.B. Berestecky, E.M. Lifshitz and L.P. Pitaevsky, Quantum Electrodynamics (Nauka, Moscow, 1989)

[16] L.A. Veinstein. Open Resonators and Wave guides (Moscow, Sovetskoye Radio, 1966)

[17] Wissenschaftlicher Jahresbericht 1993 (ISSN 0179-9282, DESY, 1993), Voruntersuchungen zu einem "Linear Collider" - Projekt, p.207

[18] A.G. Fox and T. Li, Bell Syst.Tech.J. **40**(1961)453

[19] Y.A. Anan'ev, Optical Resonators and Laser beams (Moscow, Nauka, 1990)

[20] M. Born and E. Wolf, Principles of Optics (Pergamon Press, 1968)

[21] S. Solimeno, B.Crosignani, P. DiPorto, Guiding, Diffraction and Confinement of Optical Radiation (Academic Press, INC, 1986)